# WEAK LOCALIZATION IN THIN FILMS
## a time-of-flight experiment with conduction electrons

**Gerd BERGMANN**

*IFF der KFA, Postfach 1913, 517 Jülich, West-Germany*

NORTH-HOLLAND PHYSICS PUBLISHING–AMSTERDAM

PHYSICS REPORTS (Review Section of Physics Letters) 107, No. 1 (1984) 1–58. North-Holland, Amsterdam

# WEAK LOCALIZATION IN THIN FILMS
## a time-of-flight experiment with conduction electrons

Gerd BERGMANN

*IFF der KFA, Postfach 1913, 517 Jülich, West-Germany*

Received 15 November 1983

*Contents:*



*Abstract:*

The resistance of two-dimensional electron systems such as thin disordered films shows deviations from Boltzmann theory, which are caused by quantum corrections and are called "weak localization". Theoretically weak localization is originated by the Langer–Neal graph in the Kubo formalism. In this review article the physics of weak localization is discussed. It represents an interference experiment with conduction electrons split into pairs of waves interfering in the back-scattering direction. The intensity of the interference (integrated over the time) can be easily measured by the resistance of the film. A magnetic field introduces a magnetic phase shift in the electronic wave function and suppresses the interference after a "flight" time proportional to $1/H$. Therefore the application of a magnetic field allows a time-of-flight experiment with conduction electrons. Spin–orbit scattering rotates the spin of the electrons and yields an observable destructive interference. Magnetic impurities destroy the coherence of the phase. The experimental results as well as the theory is reviewed. The role of the spin–orbit scattering and the magnetic scattering are discussed. The measurements give selected information about the inelastic lifetime of the conduction electrons in disordered metals and raise new questions in solid state physics. Future applications of the method of weak localization are considered and expected.

## 1. Introduction

During the past few years a new field in solid state physics has been theoretically and experimentally explored. It deals with the anomalous transport properties of electrons in disordered systems. The phenomenon is generally called weak localization and it is essentially caused by quantum-interference of the conduction electrons on the defects of the systems. Therefore I will also call it alternatively at times "QUIAD" (quantum-interference at defects). This phenomenon had been first considered by Abrahams et al. [1] when they developed a scaling theory for two-dimensional conductors. In their work weak localization was only an asymptotic case of a more general theory. But soon it became a field on its own with growing importance. During the mean-time extensive theoretical work [2–84] as well as experimental investigations on metals [85–128] (thin films) and [129–134] (one- and three-dimensional metals) and MOS inversion layers and other semiconductors [135–153] have followed. In particular the resistance anomaly at low temperature and the magneto-resistance have been intensively studied.

Weak localization exists in one, two and three dimensions as well but for an experimental investigation the two-dimensional case is the most favourable one. Here the correction to the resistance is of the order of $10^{-2}$ to $10^{-3}$ and can be easily measured with an accuracy of 1%. One can in particular investigate the QUIAD in two dimensions in a magnetic field perpendicular to the film (which is not possible in one dimension). We will see that the response to a magnetic field is a powerful method to determine characteristic times of the electron system. The physical reason is that weak localization corresponds to a time-of-flight experiment with conduction electrons. Therefore most of the experimental work on metals is done in thin films. Another two-dimensional electronic system has been experimentally investigated as well – electron inversion layers. Since many properties of the electronic system in inversion layers are quite different from the metal I leave the discussion of inversion layers to an expert in that field and concentrate here on two-dimensional thin films.

Since one can prepare thin films of every metal and most alloys QUIAD allows to study many materials with quite different properties such as simple metals, transition metals, superconductors, nearly magnetic metals, etc. The experimental investigation is only at the beginning but in the past it has been shown that weak localization exists, can be well described by the theory and allows to measure characteristic times of the electron system such as inelastic lifetime, spin–orbit scattering time and magnetic scattering time. However, the use of this new method has just been started, there is no systematic investigation of the large variety of materials yet.

The aim of this article is to introduce the reader into the physics of QUIAD. Section 2 concentrates on the physics of weak localization (it is essentially an extended version of a lecture the author used to deliver on weak localization). Here the complicated Kubo graph of the theory is translated into a simple physical picture. It is shown that weak localization is a rather sophisticated but transparent interference experiment.

Section 3 deals with the theory of weak localization, repeats shortly the Kubo formalism and evaluates the Langer–Neal graph in some detail. Although being a theoretical section it is written for the interested experimentalist. The plan for this section was stimulated from the difficulties which the author had with several theoretical papers in this field because they were so condensed. In particular it was often rather difficult to modify the theoretical calculations which is for example necessary if one wants to generalize a strictly two-dimensional calculation to a film of finite thickness. The large amount of non-economic work which I had to invest into some of the theoretical papers to read between the lines lead me to the conclusion that an extended section on the theory might be of some use for other interested experimentalists. Theoreticians are referred to the review articles by Fukuyama [76] and Altshuler and Aronov [154].

Since the formulae which the theory derives are not really transparent section 4 gives a graphic evaluation of these formulae to show the structure of the theory.

Section 5 describes and collects the experimental results on magneto-resistance, temperature dependence, electric field dependence, magnetic scattering, etc.

One of the most interesting experimental results of QUIAD is the measurement of the inelastic lifetime. The theoretical aspects as well as the experimental results are discussed in section 6.

Since the Coulomb interaction in disordered two-dimensional electron systems yields a similar resistance anomaly with temperature as weak localization does the properties of electron–electron interaction are briefly sketched in section 7.

Finally we discuss some of the future applications of weak localization in solid state physics in section 8.

## 2. Physical interpretation of weak localization

Thin disordered metal films show resistance anomalies which were theoretically not understood until five years ago. Fig. 2.1 shows the magneto-resistance of a thin Cu-film with a thickness of 80 Å and a high degree of disorder. Its electronic mean free path is only of the order of 10 Å. The resistance (per square) changes in a magnetic field perpendicular to the film and the magneto-resistance is strongly temperature dependent. According to the classical theory the resistance should be completely field independent because the product $\omega_c\tau_0$ is (even in a field of 7 T) only of the order of $10^{-4}$ and the magneto-resistance is proportional to the square of $\omega_c\tau_0$. ($\omega_c = He/m$ = cyclotron frequency and $\tau_0$ = elastic scattering time.) The unexpected magneto-resistance is a manifestation of the new

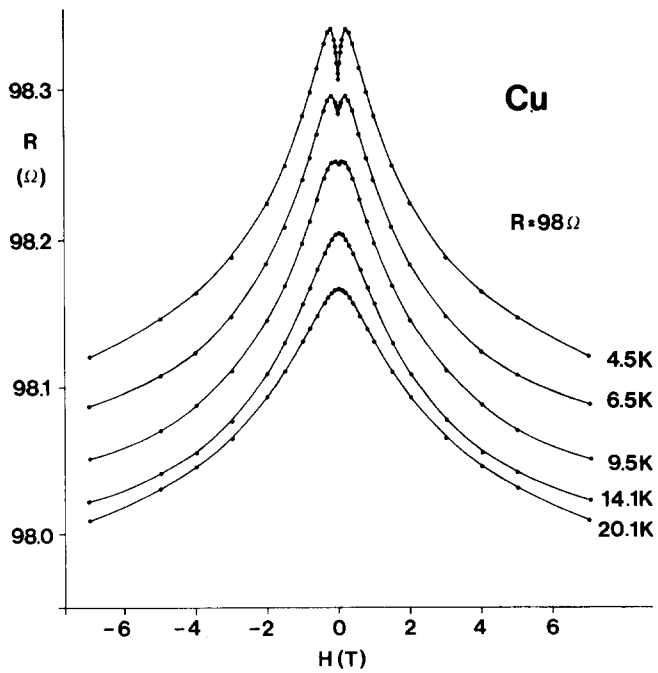


Fig. 2.1. The magneto-resistance of a thin Cu-film ($d$ = 80 Å, resistance per square $R$ = 98 Ω) at different temperatures. The mean free path is of the order of 10 Å so that classical magneto-resistance effects can be excluded.

phenomenon which is generally called weak localization. In this section we want to point out that weak localization corresponds to an interference experiment with conduction electrons which are scattered at impurities [155]. The application of a magnetic field influences this interference and introduces a time scale into the system. Finally we will recognize that the magnetic field allows to observe the fate of the conduction electrons as a function of time.

At low temperature one has to distinguish between two different lifetimes of the conduction electrons, the elastic lifetime $\tau_0$ and the inelastic lifetime $\tau_i$. Here $\tau_0$ is the lifetime of the electron in an eigenstate of momentum, whereas $\tau_i$ is the lifetime in an eigenstate of energy. At 4 K, the latter can exceed the former by several orders of magnitude. As a consequence, a conduction electron in state $k$ can be scattered by impurities without loosing its phase coherence. Due to the statistical distribution of the impurities, the multiple scattered waves form a chaotic pattern. The usual Boltzmann theory neglects interferences between the scattered partial waves and assumes that the momentum of the electron wave disappears exponentially after the time $\tau_0$ (or $\tau_{tr}$ = transport mean free path. In the following consideration we assume s scattering so that $\tau_0$ and $\tau_{tr}$ are equal). This assumption yields for free electrons the simple Drude formula for the conductivity

$$\sigma = \frac{ne^2}{m}\tau_0 . \tag{2.1}$$

The neglect of the interference is, however, not quite correct. There is a coherent superposition of the scattered electron wave which results in back-scattering of the electron wave and lasts as long as its coherence is not destroyed. This causes a correction to the conductance which is generally calculated in the Kubo formalism by evaluating "Kubo graphs". The most important correction has already been discussed by Langer and Neal [156] in 1966 and is shown in fig. 2.2a. This Langer–Neal graph has been evaluated by Abrahams et al. [1] for two-dimensional disordered systems of finite size and they concluded that a two-dimensional conductor with a finite concentration of defects becomes an insulator at $T = 0$ K. Anderson et al. [2] and Gorkov et al. [4] showed that at low but finite temperature the conductance has a correction

$$\Delta L = -\Delta R/R^2 = L_{00}\log(\tau_i/\tau_0) ; \qquad L_{00} = e^2/(2\pi^2\hbar) . \tag{2.2}$$

This correction is temperature dependent because the inelastic lifetime depends on the temperature (for example $1/\tau_i \propto T^p$). In the following we will translate the Langer–Neal graph into a transparent physical picture and show that it corresponds to an interference experiment.

### *2.1. The echo of a scattered conduction electron*

We consider at the time $t = 0$ an electron of momentum $\boldsymbol{k}$ which has the wave function $\exp[i\boldsymbol{kr}]$. The electron in state $\boldsymbol{k}$ is scattered after the time $\tau_0$ into a state $\boldsymbol{k}'_1$, after $2\tau_0$ into the state $\boldsymbol{k}'_2$, etc. There is a finite probability that the electron will be scattered into the vicinity of the state $-\boldsymbol{k}$; for example after $n$ scattering events. This scattering sequence (with the final state $-\boldsymbol{k}$)

$$\boldsymbol{k} \to \boldsymbol{k}'_1 \to \boldsymbol{k}'_2 \to \cdots \to \boldsymbol{k}'_{n-1} \to \boldsymbol{k}'_n = -\boldsymbol{k}$$

is drawn in fig. 2.2b in $k$-space. The momentum transfers are $\boldsymbol{g}_1, \boldsymbol{g}_2, \ldots, \boldsymbol{g}_n$. There is an equal

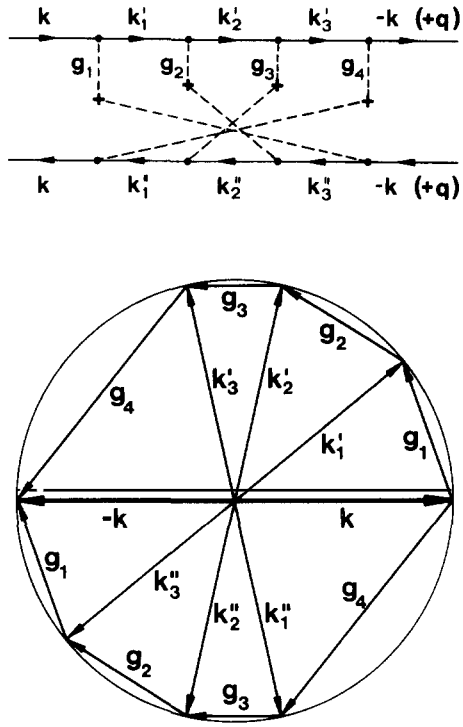


Fig. 2.2. (a) The fan diagram, introduced by Langer and Neal, which allows calculations of quantum corrections to the resistance within the Kubo formalism. (b) The physical interpretation of the fan diagram in (a). The electron in the eigenstate of momentum $k$ is scattered via two complementary series of intermediate scattering states $k \to k'_1 \to k'_2 \to \cdots \to k'_{n-1} \to k'_n = -k$ and $k \to k''_1 \to k''_2 \to \cdots \to k''_{n-1} \to k''_n = -k$ into the state $-k$. The change of momentum is $g_1, g_2, \ldots, g_{n-1}, g_n$ for the first series and $g_n, g_{n-1}, \ldots, g_2, g_1$ for the second. The amplitudes in the final state $-k$ are identical, $A' = A'' = A$ and interfere constructively, yielding an echo in back-scattering direction which decays as $1/t$ in two dimensions. Only for times longer than the inelastic lifetime $\tau_i$ the coherence is lost and the echo disappears.

probability for the electron $k$ to be scattered in $n$ steps from the state $k$ into $-k$ via the sequence

$$k \to k''_1 \to k''_2 \to \cdots \to k''_{n-1} \to k''_n = -k$$

where the momentum transfers are $g_n, g_{n-1}, \ldots, g_1$. This complementary scattering series has the same changes of momentum in opposite sequence. If the final state is $-k$, then the intermediate states for both scattering processes lie symmetric to the origin. The important point is that the amplitude in the final state $-k$ is the same for both scattering sequences. This is caused essentially by the proportionality of the final amplitude to the product of the matrix elements i.e. $\Pi\, V(g_i)$ – where $V(g_i)$ is the Fourier component of the scattering potential – and this product is the same for both sequences. Secondly the transition probability is identical because of the symmetry of the two complementary processes. In addition the energy of the corresponding intermediate states is (by pairs) the same so that the time-dependent phase changes ($Et/\hbar$) are identical.

Since the final amplitudes $A'$ and $A''$ are phase coherent and equal, $A' = A'' = A$, the total intensity is $|A' + A''|^2 = |A'|^2 + |A''|^2 + A'^* A'' + A' A''^* = 4|A|^2$. If the two amplitudes were not coherent then the total scattering intensity of the two complementary sequences would only be $2|A|^2$. This means that the scattering intensity into the state $-k$ is by $2|A|^2$ larger than in the case of incoherent scattering. This

additional scattering intensity exists only in the back-scattering direction. For other states at the Fermi surface, sufficiently far away from $-\boldsymbol{k}$, there is only an incoherent superposition of every two sequences (with momentum transfer in the opposite sequence) and therefore as an average the scattering intensity per sequence with $n$ scattering processes is only $|A|^2$.

The fan diagram in fig. 2.2a gives just the product $A'^*A''$, i.e. the interference intensity. It consists of two parts, the upper electron propagator and the lower hole propagator. The upper one yields the amplitude of the electron $\boldsymbol{k}$ which is scattered into the state $-\boldsymbol{k}$ via the scattering sequence ('). If we invert the direction of the arrows for the lower propagator then it yields the amplitude of the electron $\boldsymbol{k}$ which is scattered into the state $-\boldsymbol{k}$ via the scattering sequence (''). The reversed direction of the arrows (i.e. that it is a hole propagator) yields the complex conjugate of the amplitude.

At high temperature the scattering processes are partially inelastic. As a consequence the amplitudes $A'$ and $A''$ loose their phase coherence (after the time $\tau_i$) and the intensity of the back-scattered wave is only $2|A|^2$, i.e. the coherent back-scattering disappears after the time $\tau_i$. In fig. 2.3 the momentum of the electron $\boldsymbol{k}$ is plotted as a function of time. The original momentum decays within the elastic lifetime $\tau_0$. At later times a momentum in the opposite direction is formed; this decreases inversely proportional to the time (as we shall see below). One obtains an echo of the original state $\boldsymbol{k}$ in opposite direction which vanishes only when the two processes loose their coherence. Obviously the integrated momentum of the electron $\boldsymbol{k}$ decreases with increasing $\tau_i$. In the following we treat this scattering semi-quantitatively.

After the elastic lifetime $\tau_0$ the electron $\boldsymbol{k}$ is scattered into a shell at the Fermi surface which is assumed to contain $Z$ intermediate states. The amplitude in the intermediate state $\boldsymbol{k}_1'$ is $Z^{-1/2}\,e^{i\delta_1}$ where $e^{i\delta_1}$ is essentially given by $V(\boldsymbol{g}_1)/|V(\boldsymbol{g}_1)|$. The intensity in the next intermediate state $\boldsymbol{k}_2'$ at the time $2\tau_0$ is $Z^{-2}$. After $n$ scattering processes the intensity in the final state $-\boldsymbol{k}$ is $Z^{-n}$ and the amplitude $Z^{-n/2}\,e^{i\sum\delta_\nu}$. The second scattering series yields the same amplitude. The cross product or interference term is $A'^*A'' + A'A''^* = 2Z^{-n}$. Now we have to sum over all possible intermediate states. This yields the factor $1/2\,Z^{n-1}$. (1/2 occurs because the two complementary series appear twice in the sum.) Therefore the coherent additional back-scattering intensity is $Z^{-1}$. It is independent of the number of intermediate scattering states $n$ and equal to the scattering intensity from $\boldsymbol{k}$ into $\boldsymbol{k}_1'$. This intensity is, of course, completely calculated in evaluating the diagram with the appropriate rules. However, one can easily estimate this intensity in a rather direct and less formal manner.

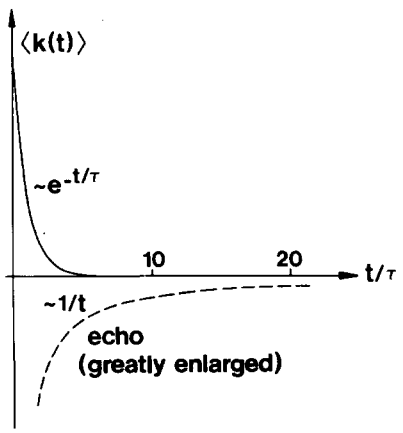


Fig. 2.3. The contribution of the electron state $\boldsymbol{k}$ to the momentum as function of time. The original state and its momentum decay exponentially within the time $\tau_0$ (s scattering assumed). But an echo with the momentum $-\boldsymbol{k}$ is formed which depends on time as $1/t$. This echo reduces the contribution of the electron to the current and yields a correction to the resistance which is proportional to $\log(\tau_i/\tau_0)$.

For the calculation of $Z$ in two dimensions we consider the scattering from the state $\boldsymbol{k}$ into the state $\boldsymbol{k}'_1$. This state is an intermediate state for the scattering sequence which does not have to conserve the energy (sometimes called virtual scattering process). Since the elastic lifetime is $\tau_0$ the intermediate state can lie within $\pi\hbar/\tau_0$ of the Fermi energy. This corresponds to a smearing of the Fermi sphere by $\pi/l$ ($l$ = mean free path of the conduction electrons). Therefore the available area in $k$-space is $2\pi k_F * \pi/l = 2\pi^2 k_F/l$ and $Z$ is obtained by multiplying by the density of state in $k$-space, i.e. $(2\pi)^{-2}$.

The coherent back-scattering is not restricted to the exact state $-\boldsymbol{k}$; one has a small spot around the state $-\boldsymbol{k}$ in momentum space which contributes. We calculate the coherent back-scattering intensity into the state $-\boldsymbol{k}+\boldsymbol{q}$ which is reached after $n$ scattering processes with the transfer of momentum $\boldsymbol{g}_i$ where $\Sigma \boldsymbol{g}_i = -2\boldsymbol{k}_F + \boldsymbol{q}$. The sum of the momenta of the initial and final state is $+\boldsymbol{q}$. The same applies for each pair of scattering states in fig. 2.2b which lie opposite to the centre, i.e. $\boldsymbol{q} = \boldsymbol{k}'_1 + \boldsymbol{k}''_{n-1} = \boldsymbol{k}'_2 + \boldsymbol{k}''_{n-2} = \ldots$ The corresponding intermediate states differ not only in momentum but also in energy (which must not be conserved). The energy difference is $\hbar\boldsymbol{q} * \boldsymbol{v}_F$ and since the phase rotates with $Et/\hbar$ one obtains during the time $\tau_0$ a phase difference between the two complementary waves which is $\boldsymbol{q} * \boldsymbol{v}_F\tau_0$. The important fact is that the different intermediate states have independent directions of momentum. Therefore the phase differences are independent in sign and value. This means that only the square of the phase shifts adds. Therefore after the $n$ scattering processes one obtains phase differences between the complementary waves whose width is

$$[\Delta\varphi]^2 = n\overline{(\boldsymbol{q} * \boldsymbol{v}_F\tau_0)^2} = n\,\tfrac{1}{2}(v_F q\tau_0)^2 = nDq^2\tau_0\,. \tag{2.3}$$

In two dimensions the average over $(\boldsymbol{v}_F * \boldsymbol{q})^2$ is $(v_F q)^2/2$ (and in three dimensions $(v_F q)^2/3$ but the diffusion constant absorbs the factor of dimension). The neighbouring states of $-\boldsymbol{k}$ contribute less to the coherent back-scattering because they loose the phase coherence with increasing $n$ and $q$. Their contribution is proportional to $\exp[-Dq^2t]$ since $t = n\tau_0$. The area of the spot for the coherent back-scattering is obtained by integration over $\boldsymbol{q}$. In two dimensions this yields $\pi/(Dt)$. This corresponds to about $\pi(Dn\tau_0)^{-1}/(2\pi)^2$ states, i.e. their number shrinks with time. Therefore the portion of coherent back-scattering is given by

$$I_{coh} = [\pi/(Dt)]/[2\pi^2 k_F/l] = \tau_0/(\pi k_F l t) = \hbar/(2\pi E_F t)\,. \tag{2.4}$$

In the presence of an external electrical field the conduction electrons contribute to the current. However, the echo, i.e., the coherent back-scattering reduces the current and therefore the conductance. A pulse of an electrical field generates a short current (for the time $\tau_0$) in the direction of the electric field and then a reversed current which decays as $1/t$. The dc conductance is obtained by integrating the momentum over time. For the normal contribution this yields $\boldsymbol{k}\tau_0$ and for the echo $[\boldsymbol{k}\tau_0/(\pi k_F l)]\ln(\tau_i/\tau_0)$. Therefore the electron in the state $\boldsymbol{k}$ contributes to momentum

$$\boldsymbol{k}\tau_0\{1 - [1/(\pi k_F l)]\ln(\tau_i/\tau_0)\}\,. \tag{2.5}$$

The contribution of the electron $\boldsymbol{k}$ to the current is reduced by the factor in the brackets and the conductance is decreased by the same factor,

$$\begin{aligned} L &= (ne^2\tau_0/m) * \{1 - [1/(\pi k_F l)]\ln(\tau_i/\tau_0)\} \\ &= (ne^2\tau_0/m) - [e^2/(2\pi^2\hbar)] * \ln(\tau_i/\tau_0) \end{aligned} \tag{2.6}$$

with $n = 2\pi k_F^2/(2\pi)^2$. This correction to the conductance was introduced by Anderson et al. [2] and Gorkov et al. [4].

The important consequence of the above consideration is that the conduction electrons perform a typical interference experiment. The (incoming) wave $\boldsymbol{k}$ is split into two complementary waves $\boldsymbol{k}_1'$ and $\boldsymbol{k}_1''$. The two waves propagate individually, experience changes in phase, spin orientation, etc. and are finally unified in the state $-\boldsymbol{k}$ where they interfere. The intensity of the interference is simply measured by the resistance. In the situation which has been discussed above the interference is constructive in the time interval from $\tau_0$ to $\tau_i$. It is only slightly more complicated than a usual interference experiment because one has a larger number of pairs of complementary waves.

Shortly after the development of the theory several experimental groups investigated the resistance of thin disordered films (and MOS inversion layers) as a function of temperature and found indeed an increase of the resistance with the logarithm of the (decreasing) temperature. Figs. 2.4a–c show results by Dolan and Osheroff [85] on thin AuPd-films, and Van den dries et al. [87] and Kobayashi et al. [86] on thin Cu-films. These experimental results appeared to be an experimental proof of the theory of weak localization. However, a few months later Altshuler et al. [157] showed that there is another effect in two-dimensional disordered systems which causes essentially the same resistance anomaly with temperature. They showed that in disordered electron systems the Coulomb interaction is modified. The electron–electron interaction is dynamically not perfectly screened but long ranged. This has an important impact on the density of states as well as on the resistance of disordered two-dimensional electron systems. We shall return to the effect of the Coulomb interaction in section 7. As a consequence of this alternative mechanism one had to look for a more characteristic experimental investigation of weak localization. The application of a magnetic field provided such a possibility.

## 2.2. *Time-of-flight experiment in a magnetic field*

One of the interesting possibilities for an interference experiment is to shift the relative phase of the two interfering waves. For charged particles this can be easily done by an external magnetic field.

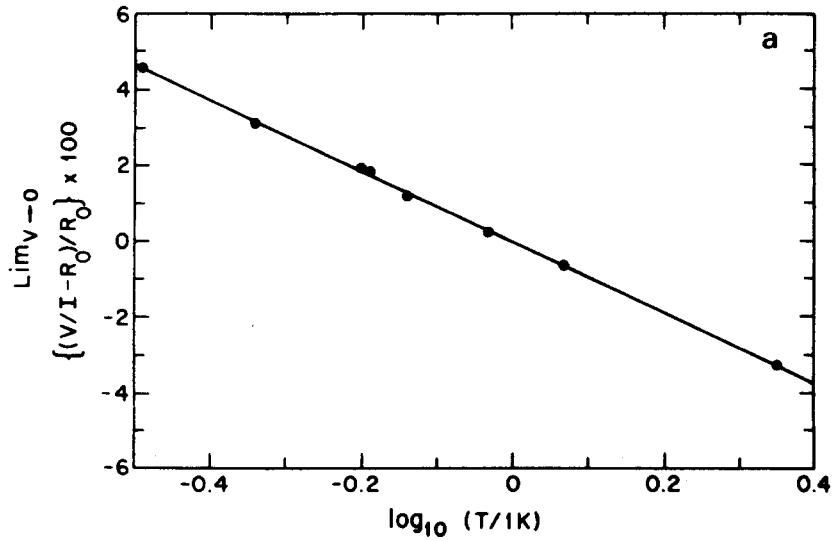


Fig. 2.4(a).

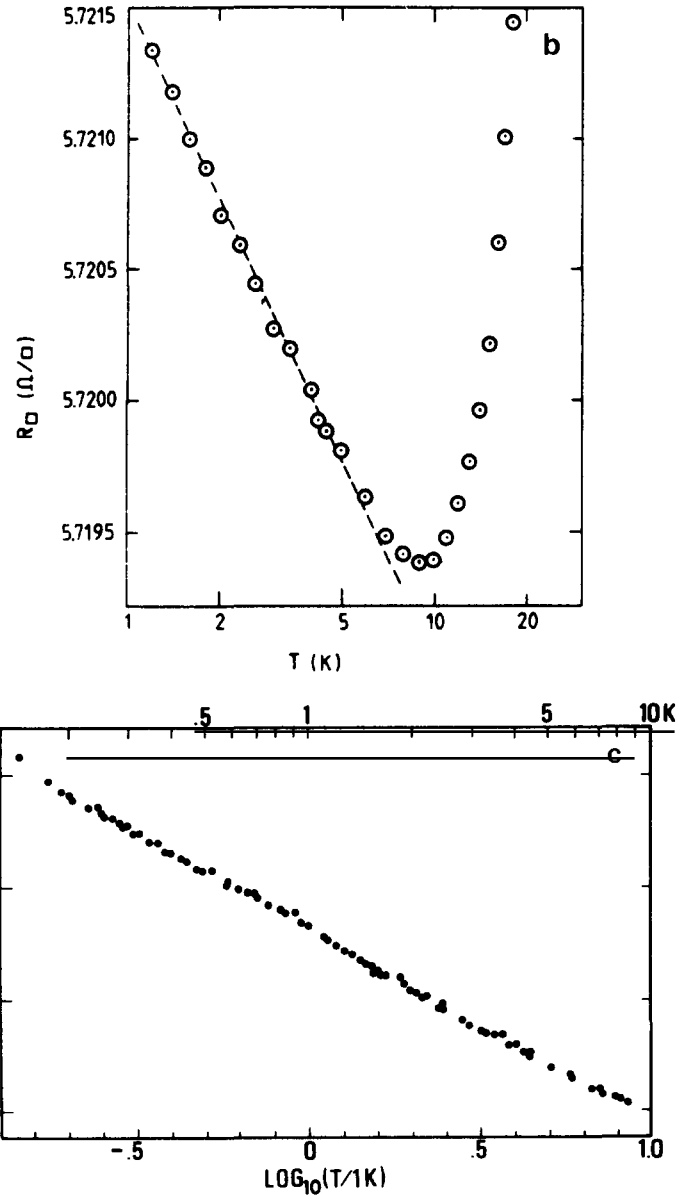


Fig. 2.4. The resistance of thin disordered films as function of the logarithm of the temperature. (a) a AuPd-film by Dolan and Osheroff [85], (b) a Cu-film by Van den dries et al. [87] and (c) coupled fine Cu-particles by Kobayashi et al. [86].

Before we treat the effect of a magnetic field in some detail we consider the motion of the conduction electron in real space. Since the conduction electron has a very short mean free path it diffuses in the two-dimensional conductor from impurity to impurity. Consider an electron at the origin at $t = 0$. The classical diffusion equation in two dimensions yields for the probability (density) of finding the electron at the time $t$ at the position $\boldsymbol{r}$

$$p(\boldsymbol{r}, t) = [1/(4\pi Dt)] * \exp[-r^2/(4Dt)] . \tag{2.7}$$

The chance to return to the origin is given by $1/(4\pi Dt)$. In fig. 2.5 a possible path is drawn for the diffusion of an electron which returns to the origin. For classical diffusion one has an identical probability for the electron to propagate on the same path in the opposite direction. The two probabilities add up and contribute to the total probability of $1/(4\pi Dt)$. Since the electron has wave-like character in reality one has to consider two partial waves of the electron which propagate in opposite directions on the indicated path. Returned to the origin, however, their amplitudes add (instead of their intensities). It is the same physical mechanism which has been discussed in momentum space before. This picture has been used by Altshuler et al. [26] in studying the electric field effect on QUIAD. The amplitudes $A'$ and $A''$ are equal because their partial waves propagated on the same path in opposite directions and as long as the system shows time reversal the two partial waves arrive at the origin in phase and with the same amplitude. Therefore the intensity or probability is twice as large as in the classical diffusion problem i.e. $1/(2\pi Dt)$. For the diffusion to any other point except the vicinity of the origin the different partial waves are generally incoherent and only their intensities add. (There is only a small reduction to compensate the increased intensity at the origin.) In fig. 2.6 the classical and the quantum diffusion probabilities are plotted qualitatively. The (dashed) peak in quantum diffusion at the origin describes a tendency to remain at or return to the origin. Since it is thought of as a precursor of localization this quantum diffusion has been called weak localization. (A localized electron would

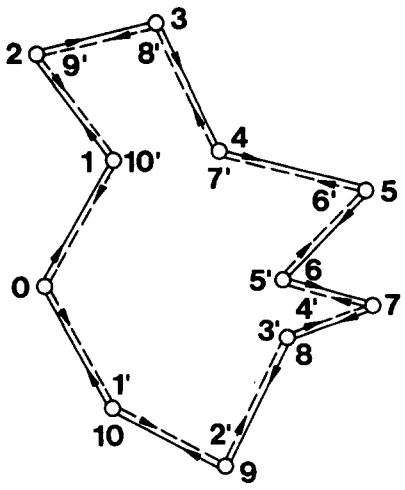


Fig. 2.5. Diffusion path of the conduction electron in the disordered system. The electron propagates in both directions (full and dashed lines). In the case of quantum diffusion the probability to return to the origin is twice as great as in classical diffusion since the amplitudes add coherently.

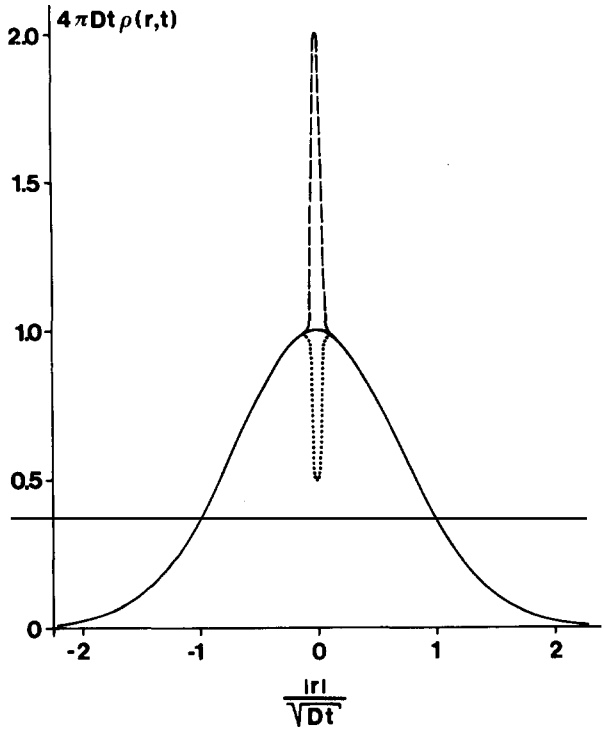


Fig. 2.6. The probability distribution of a diffusing electron which starts at $r = 0$ at the time $t = 0$. In quantum diffusion (dashed peak) the probability to return to the origin is twice as great as in classical diffusion (full curve). Large spin–orbit scattering reduces the probability by a factor of two (dotted peak) and yields a weak anti-localization.

remain close to the origin.) This name is, however, questionable because in the presence of large spin–orbit scattering – as we discuss below – the quantum diffusion yields a reduced probability (dotted peak) to return to the origin, an effect one might call weak anti-localization [46].

In a magnetic field, however, the phase coherence of the two partial waves is weakened or destroyed. When the two partial waves surround an area $F$ containing the magnetic flux $\phi$, then the relative change of the two phases is $(2e/\hbar)\phi$. The factor of 2 arises because the two partial waves surround the area twice. (This is sometimes interpreted as if a particle with twice the electron charge surrounds the area in analogy to the double charge $2e$ in superconductivity.)

Since the diffusion is statistical for a given diffusion time $t$ a whole range of enclosed areas for the different diffusion paths exists. Altshuler et al. [19] suggested performing such an "interference experiment" with a cylindrical film in a magnetic field parallel to the cylinder axis. Then the magnetic phase shift between the complementary waves is always a multiple of $2e\phi/\hbar$ ($\phi$ = flux in the area of the cylinder). Sharvin and Sharvin [92, 102] showed in a beautiful experiment that then the resistance oscillates with a flux period of $\phi = h/(2e)$. Fig. 2.7a shows the geometry of a thin cylindrical film and fig. 2.7b the oscillation of the resistance for a thin cylindrical Mg-film [92].

However, for a thin film in a perpendicular magnetic field the pairs of partial waves enclose areas between $-2Dt$ and $2Dt$. When the largest phase shift exceeds 1, the interference is both constructive and destructive as well and the average cancels. This happens roughly after the time $t_H = \hbar/(4eDH)$. This means essentially that the conductance correction in the field $H$ i.e. $\Delta L(H)$ yields the coherent back-scattering intensity by integrating from $\tau_0$ to $t_H$

$$\Delta L(H) \propto \int_{\tau_0}^{t_H} I_{\mathrm{coh}}\, \mathrm{d}t \propto -L_{00} \log(t_H/\tau_0)\,. \tag{2.8}$$

It is important to mention that only the amplitudes of the "scattered" waves interfere. There is no interference between the original wave function and its scattered component considered in this theory and at these finite temperatures the coherence length, i.e. the length over which a wave packet can be defined at finite temperature and which is of the order of $\hbar v_F/(k_B T)$ is much smaller than the inelastic mean free path $v_F\tau_i$. (Otherwise one is no longer in the region of QUIAD.)

The quantitative calculation yields a simple result. The application of a magnetic field causes a destructive interference in the final state $-\boldsymbol{k}$. But in the vicinity of $-\boldsymbol{k}$ for the states $-\boldsymbol{k}+\boldsymbol{q}$ the interference is constructive if $\boldsymbol{q}$ lies on Landau-like circles with $(\hbar q)^2/(4m) = \hbar\omega_c(n+\frac{1}{2})$ where $\omega_c$ is the cyclotron frequency. The allowed states as a function of $\boldsymbol{q}$ are shown in fig. 2.8. (The electron states on the "Landau circles" are not free electron states in a magnetic field because they are centred around $-\boldsymbol{k}$. Only formally they correspond to hypothetical particles with twice the electron mass.) Since, on the other hand, the width of the coherently back-scattered spot shrinks with time as $(Dt)^{-1/2}$ the coherent back-scattering dies out when the spot lies completely inside the first Landau circle with the radius $(2eH/\hbar)^{1/2}$. This occurs for fields of the order of $H = \hbar/(4eDt)$.

This means that the magnetic field allows a time-of-flight experiment. If a magnetic field $H$ is applied the contribution of coherent back-scattering is integrated in the time interval between $\tau_0$ and $t_H = \hbar/(4eDH)$. If one reduces the field from the value $H'$ to the value $H''$ and measures the change of resistance this yields the contribution of the coherent back-scattering in the time interval $t_{H'}$ and $t_{H''}$. In a very strong field the coherent interference is suppressed. A reduction of the field integrates the coherent back-scattering and increases the resistance. If $t_H$ exceeds the inelastic lifetime of the

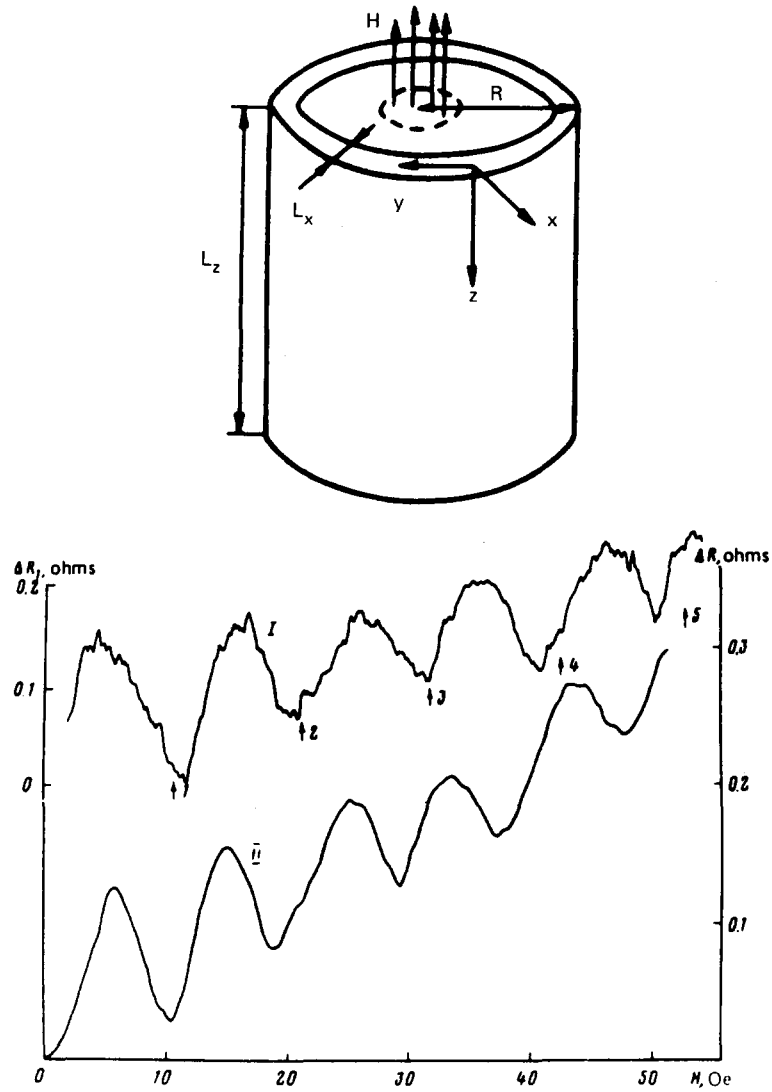


Fig. 2.7. Aranov–Bohm effect in a disordered hollow cylinder in a magnetic field parallel to the cylinder axis as suggested by Altshuler and Aronov [19], (a) the geometry, (b) the resistance oscillation as a function of the applied magnetic field measured by Sharvin and Sharvin [92] on a cylindrical Mg-film.

conducting electrons, i.e. $H < H_i = \hbar/(4eD\tau_i)$ then the coherence is lost anyway and the magneto-resistance disappears. Since the magnetic field introduces a time $t_H$ into the electron system all characteristic times $\tau_n$ of the electrons can be expressed in terms of magnetic fields $H_n$,

$$\tau_n \Leftrightarrow H_n \tag{2.9}$$

where $\tau_n H_n = \hbar/(4eD)$. In a thin film this is given by $\hbar e\rho N/4$ which is of the order of $10^{-12}$ to $10^{-13}$ Ts ($\rho$ = resistivity of the film and $N$ = density of electron states for both spin directions). A magnetic field of 1 T corresponds to about 0.1–1 ps, i.e. the magneto-resistance measurement allows picosecond

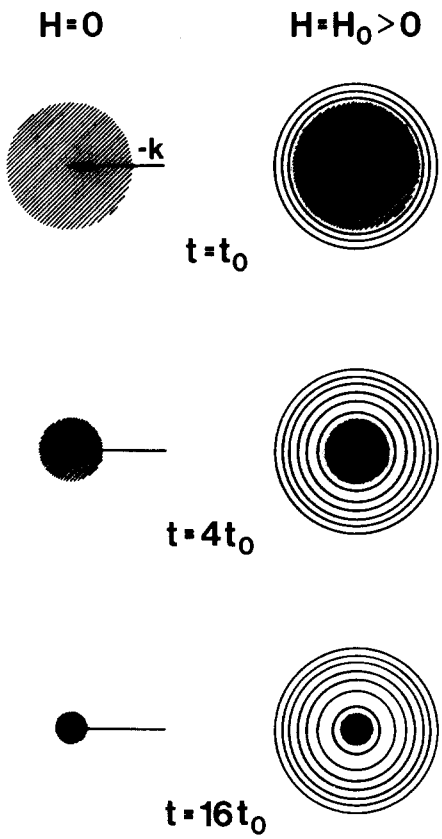


Fig. 2.8. The back-scattering spot (close to the state $-\boldsymbol{k}$) without magnetic field (left side) and in a finite magnetic field $H$. The spot has a finite area $\pi/(Dt)$ which shrinks with time. In a magnetic field the coherence condition is modified and only $\boldsymbol{k}$ states which lie on "Landau"-like circles allow coherent back-scattering. For long time $t$ the two interference conditions exclude each other because the spot is inside of all "Landau" circles and the coherent back-scattering dies at a time $t_H = \hbar/(4eDH)$. The resistance integrates the coherent back-scattering intensity in the time interval from $\tau_0$ to $t_H$.

spectroscopy with the conduction electrons. The exact formulae for the magneto-conductance are derived in section 3.

The motion of the conduction electron in real space gives a simple criterion for the conditions under which a thin film is two-dimensional [27, 53, 91]. The important requirement for the quantum interference is that the electron wave function is coherent. Therefore a system is two-dimensional with respect to QUIAD when its coherence volume has a two-dimensional shape. Without a magnetic field the electron diffuses during its inelastic lifetime over a distance of $(D\tau_i)^{1/2}$. If the thickness of the film is much less than this "Thouless length" then the region of coherence is two-dimensional. For films thinner than 100 Å thickness and at temperatures below 20 K this requirement is generally very well fulfilled. However, in strong magnetic fields the distance of coherent diffusion $(Dt_H)^{1/2}$ is much less and therefore one easily moves into the three-dimensional range. Therefore one expects deviations from the two-dimensional formula in high magnetic fields (one has to include the sheets in $\boldsymbol{k}$-space for $k_z = \nu * \pi/d$; $d$ = film thickness, see sections 3 and 5).

Before we turn to the evaluation of the experimental magneto-resistance curves we have to discuss the influence of the spin–orbit scattering.

## 2.3. Spin–orbit scattering

One of the most interesting questions in QUIAD is the influence of spin–orbit scattering [7, 8, 24]. Hikami et al. [7] predicted in the presence of strong spin–orbit scattering a logarithmic decrease of the resistance with decreasing temperature. As a consequence the magneto-resistance should change sign as well. This prediction is contrary to the picture of localization and was one of the most exciting questions at LT XVI. The prediction by Hikami et al. could be experimentally confirmed by the author [96]. For this purpose a thin Mg-film has been prepared in an ultra high vacuum. Mg is a light metal and has a very small spin–orbit coupling. The upper part of fig. 2.9 shows the magneto-resistance of the pure Mg-film at different temperatures. After the measurement the Mg-film has been covered with 1/100 layer of the strong spin–orbit coupler Au. This causes a significant change of the magneto-resistance as is shown in the lower part of fig. 2.9. At low temperature the magneto-resistance changes sign and shows a substructure which reflects the strength of the spin–orbit scattering. In fig. 2.10 the magneto-resistance of another Mg-film at 4.5 K is plotted for increasing coverage with Au. The points represent the experimental results, whereas the full curves are calculated with the theory of Hikami et al. The adjustable parameter is the spin–orbit scattering time which decreases with increasing Au coverage (this experiment also yields the spin–orbit scattering of the pure Mg-film). Obviously weak localization provides a new and very sensitive method to measure the spin–orbit scattering directly, i.e. with a substructure and not only by a broadening of a resonance.

Now we can turn to the evaluation of the magneto-resistance curves of pure Mg. In fig. 2.11 the magneto-resistance of a Mg-film is plotted as a function of the applied magnetic field [97]. The units of the field are shown on the right side of the curves. The Mg is quench-condensed at helium temperature,

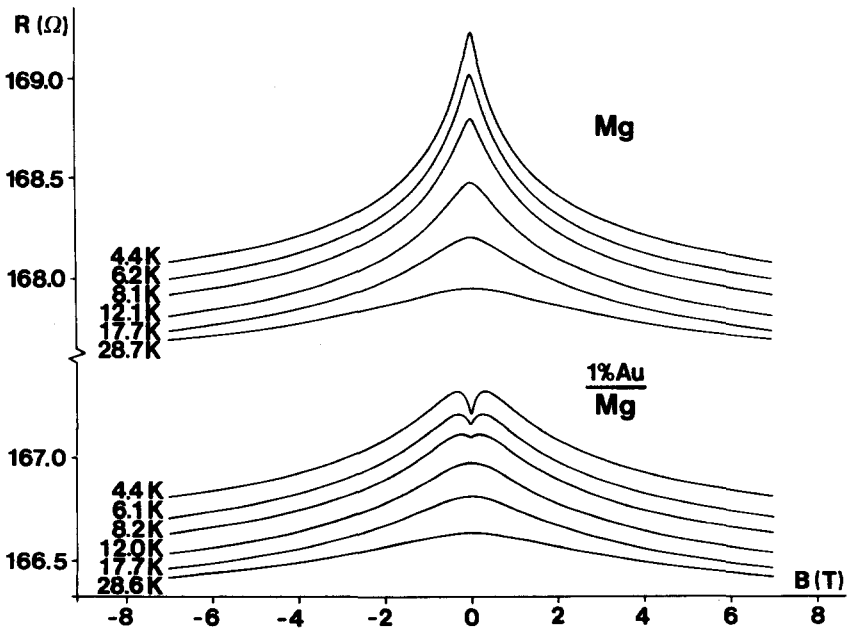


Fig. 2.9. The magneto-resistance curves of a thin Mg-film (upper set of curves). After a superposition with 1/100 atomic layer of Au the magneto-resistance changes drastically. The Au introduces a rather pronounced spin–orbit scattering which rotates the spins of the complementary scattered waves. This changes the interference from constructive to destructive.

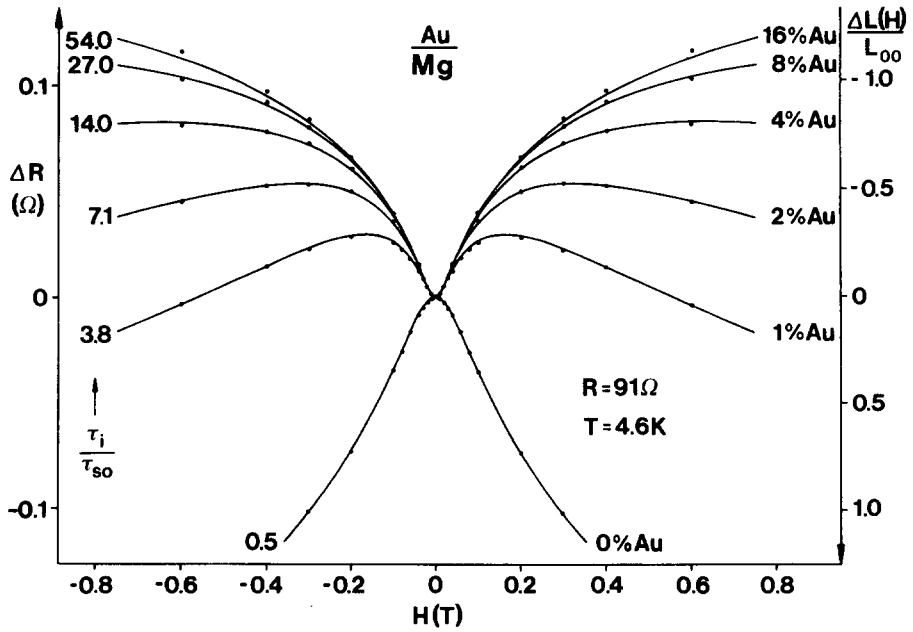


Fig. 2.10. The magneto-resistance of a thin Mg-film at 4.5 K for different coverages with Au. The Au thickness is given in % of an atomic layer on the right side of the curves. The superposition with Au increases the spin–orbit scattering. The points are measured. The full curves are obtained with the theory by Hikami et al. The ratio $\tau_i/\tau_{so}$ on the left side gives the strength of the adjusted spin–orbit scattering. It is essentially proportional to the Au-thickness.

because the quenched condensation yields homogeneous films with high resistances. The points are measured. The spin–orbit scattering of the pure Mg is determined as discussed above. The different experimental curves for different temperatures are theoretically distinguished by their different $H_i$ (i.e. the inelastic lifetime). This is the only adjustable parameter for a comparison with theory (after $H_{so}$ is determined). The ordinate is completely fixed by the theory in the universal units of $L_{00}$ (right scale). The full curves give the theoretical results with the best fit of $H_i$ which is essentially a measurement of $H_i$. The agreement between the experimental points and the theory is very good. The experimental result proves the destructive influence of a magnetic field on QUIAD. It measures the area in which the coherent electronic state exists as a function of temperature and allows the quantitative determination of the coherent scattering time $\tau_i$. The temperature dependence is given by a $T^{-2}$ law for Mg as is shown in fig. 2.12.

For other metal films where the nuclear charge is higher than in Mg one finds even in the pure case the substructure caused by spin–orbit scattering. In fig. 2.13 the magneto-resistance curves for a thin quench condensed Cu-film are shown. Again the points represent the experimental results whereas the full curves show the theory. At low temperatures the inelastic lifetime is long and therefore the effect of the spin–orbit scattering dominates in small fields. At high temperatures the inelastic lifetime becomes smaller than the spin–orbit scattering time and the magneto-resistance becomes negative because of the minor role of the spin–orbit scattering. For Au-films the spin–orbit scattering is so strong that it completely dominates the magneto-resistance.

The natural question is, why does weak localization change to weak anti-localization in the presence of spin–orbit scattering?

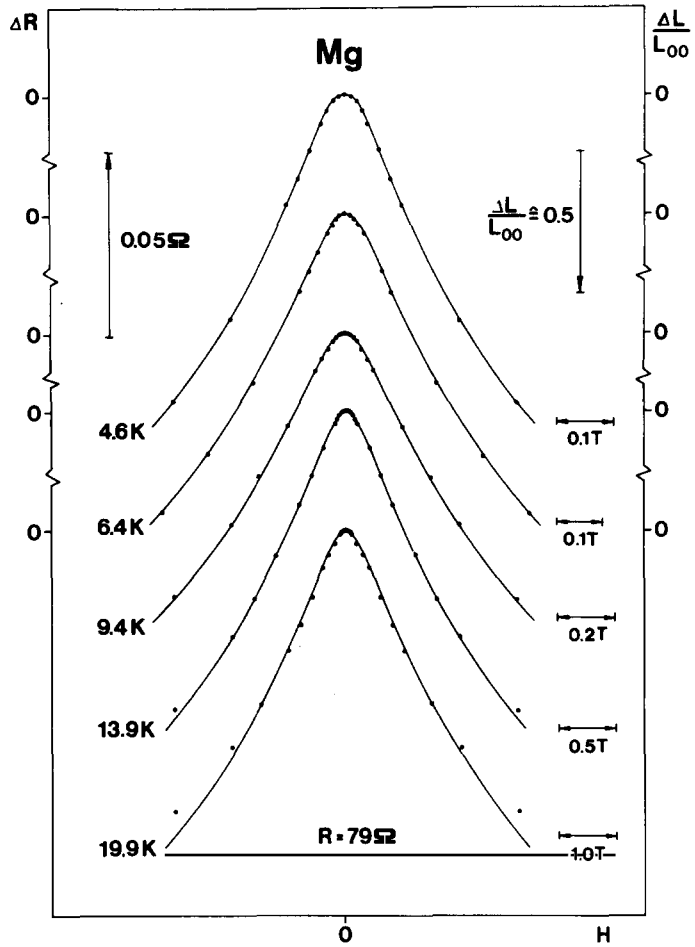


Fig. 2.11. The magneto-resistance of a thin Mg-film for different temperatures as a function of the applied field. The units of the field are given on the right of the curves. The points represent the experimental results. The full curves are calculated with the theory. The small spin–orbit scattering is taken into account.

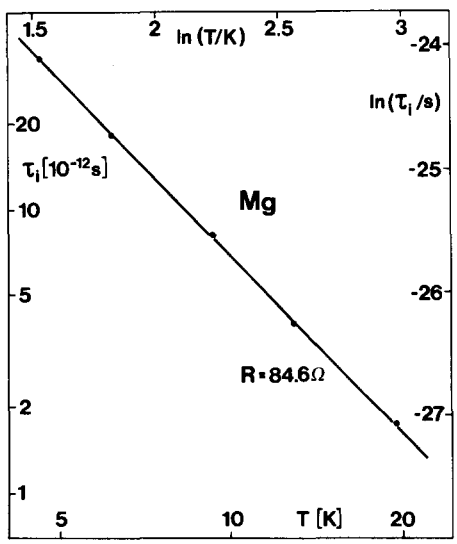


Fig. 2.12. The inelastic lifetime $\tau_i$ of a Mg-film as a function of temperature. It obeys a $T^{-2}$-law.

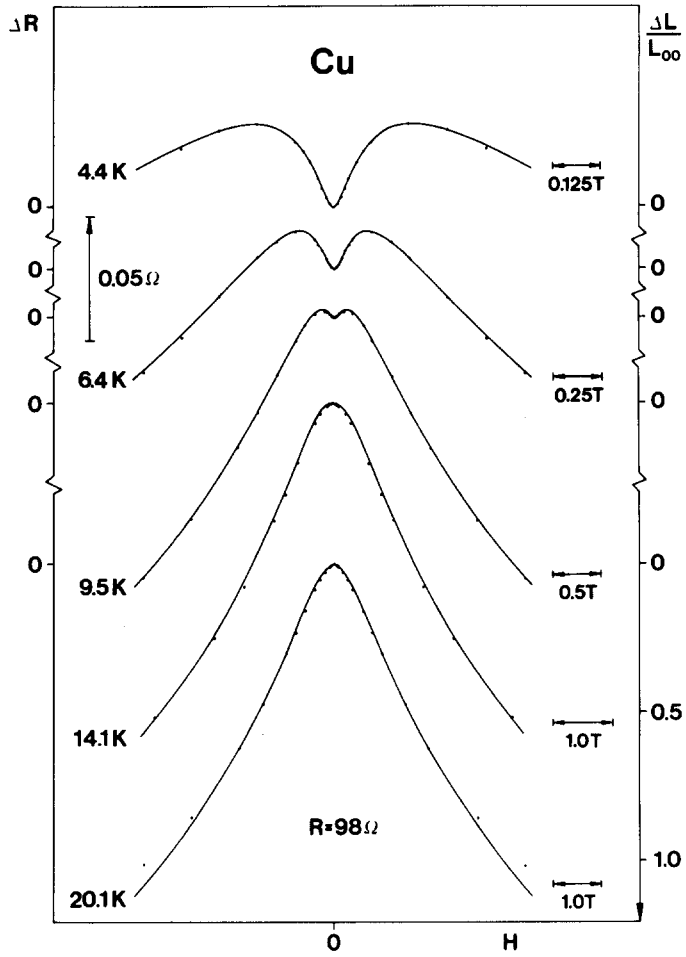


Fig. 2.13. The magneto-resistance of a Cu-film for different temperatures. The Cu possesses a natural spin–orbit scattering and therefore the pure metal shows the destructive interference of rotated spins. Again the points are experimentally measured whereas the full curves are calculated with the theory, adjusting the inelastic lifetime and the spin–orbit scattering time (expressed by the corresponding fields $H_i$ and $H_{so}$).

## 2.4. *Interference of rotated spins*

It is a consequence of quantum theory and proved by a rather sophisticated neutron experiment that spin 1/2 particles have to be rotated by $4\pi$ to transfer the spin function into itself. A rotation by $2\pi$ reverses the sign of the spin state. Weak anti-localization gives another experimental proof of this fact. In the presence of spin–orbit scattering the matrix element for a transition from state $\boldsymbol{k}$ to $\boldsymbol{k}'$ has the form

$$V_{\boldsymbol{k}-\boldsymbol{k}'}[1 - \mathrm{i}\epsilon \boldsymbol{k} \times \boldsymbol{k}' * \boldsymbol{\sigma}] \propto [1 - \mathrm{i}\boldsymbol{K} * \boldsymbol{\sigma}]\,. \tag{2.10}$$

This matrix element describes a rotation of the electron spin by the angle $K_i$ around the axis $x_i$ ($i = 1, 2, 3$). During the whole scattering series (') the spin orientation diffuses into a final state $\boldsymbol{\sigma}'$ which

can be obtained by a rotation $T$ of the original spin state $\sigma$ ($\sigma' = T\sigma$). It is straightforward to show that the finite spin state of the complementary scattering series (") is $\sigma'' = T^{-1}\sigma$. Without the spin rotation the interference of the two partial waves is constructive (in the absence of an external field). In the presence of spin–orbit scattering the interference becomes destructive if the relative rotation of $\sigma'$ and $\sigma''$ is $2\pi$. It can be shown that for strong spin–orbit scattering the destructive part exceeds the constructive one [46]. This means that the back-scattering is reduced below the statistical one. This corresponds to an echo in the forward direction and a decrease of the resistance. The magneto-resistance curve in fig. 2.9b for 1% Au on top of Mg can be interpreted as follows. In a high magnetic field where $t_H < \tau_{so}$ the spin states of the complementary states are almost unchanged and one obtains the usual negative magneto-resistance. For $t_H > \tau_{so}$ (and $t_H < \tau_i$) the interference is destructive and shows the opposite sign. For $t_H \approx \tau_{so}$ it changes sign. The resistance maximum in a finite field corresponds to a relative rotation of $\sigma'$ and $\sigma''$ by the angle $\pi$ (in an average).

### *2.5. Magnetic scattering*

Another interesting application of QUIAD is the determination of magnetic scattering by magnetic ions. The magnetic ion introduces an interaction with a conduction electron $J\,\boldsymbol{S} * \boldsymbol{\sigma}$, where $\boldsymbol{S}$ and $\boldsymbol{\sigma}$ are the ion and electron spins. The magnetic ions scatter the two complementary waves differently and destroy their coherence after the magnetic scattering time $\tau_s$ (see section 5).

## 3. Theory of the quantum corrections to the conductance

### *3.1. Kubo formalism*

The theoretical physics has involved quite some effort to develop automatic rules for the calculation of many physical properties. One example is the Kubo formalism which allows the calculation of the conductance in an electronic system. Starting with a perturbation

$$H'(t) = -\int \mathrm{d}^3x\, \boldsymbol{A}(x, t)\, j_p(x)$$

where $j_p$ is the (paramagnetic) current density

$$j_p(x) = -\frac{ie}{2m}\left[\psi^+ \nabla\psi - (\nabla\psi)\,\psi^+\right]$$

and $\boldsymbol{A}(x)$ is the vector potential where $\psi$ is the field operator. Kubo derived a $q$- and $\omega$-dependent conductance:

$$\sigma_{\mu\nu}(\boldsymbol{q}, \omega) = \mathrm{i}\int_{-\infty}^{0} \mathrm{d}t\, \langle[j_\mu(\boldsymbol{q}, 0), j_\nu(-\boldsymbol{q}, t)]\rangle \frac{\exp(\mathrm{i}\omega t)}{\mathrm{i}\omega} - \frac{ne^2}{m}\frac{1}{\mathrm{i}\omega}\delta_{\mu\nu}. \tag{3.1}$$

The current–current commutator yields electron–hole propagators as shown in fig. 3.1 (for $q = 0$):

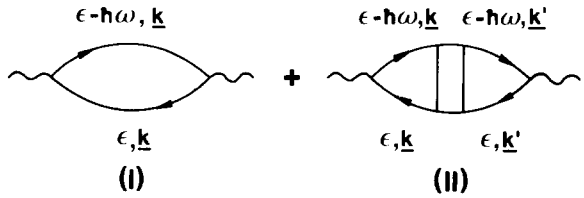


Fig. 3.1. The two Kubo graphs which contribute to the conductance in the presence of impurity scattering.

The contribution of the first diagram to the conductance is

$$\sigma_{ij}^{(\mathrm{I})}(\omega) = e^2 \int \frac{\mathrm{d}\epsilon}{2\pi} \frac{f(\epsilon - \hbar\omega) - f(\epsilon)}{\omega} \int \frac{\mathrm{d}^z k}{(2\pi)^z} \sum_\sigma v_i(\boldsymbol{k})\, v_j(\boldsymbol{k})\, G_\sigma^{\mathrm{R}}(\epsilon, \boldsymbol{k})\, G_\sigma^{\mathrm{A}}(\epsilon - \hbar\omega, \boldsymbol{k}) . \tag{3.2}$$

Here $v_i(\boldsymbol{k})$ is the $i$-component of the velocity

$$v_i(\boldsymbol{k}) = \frac{1}{\hbar} \frac{\mathrm{d}\eta(k)}{\mathrm{d}k_i} \qquad (\eta = \text{kinetic energy}) .$$

The retarded and advanced Green's functions are given by

$$\begin{aligned} G_\sigma^{\mathrm{R}}(\epsilon, k) &= \frac{1}{\epsilon + (\mathrm{i}\hbar/2\tau) - \eta(k)} \\ G_\sigma^{\mathrm{A}}(\epsilon, k) &= \frac{1}{\epsilon - (\mathrm{i}\hbar/2\tau) - \eta(k)} . \end{aligned} \tag{3.3}$$

$z$ is the dimension of the electronic system, $\tau$ is the lifetime in an eigenstate of momentum. It is essentially given by the elastic scattering time $\tau_0$ but it is important to distinguish between $\tau$ and $\tau_0$ (only in the final result one may replace $\tau$ by $\tau_0$). We shortly sketch the evaluation of $\sigma_{ij}^{(\mathrm{I})}$ because it reflects the properties of the Green's functions which are also essential for the evaluation of the quantum corrections. Generally we have to solve integrals of the form:

$$\int \frac{\mathrm{d}^z k}{(2\pi)^z} B(\boldsymbol{k})\, G^{\mathrm{R}}(\epsilon, \boldsymbol{k})\, G^{\mathrm{A}}(\epsilon - \hbar\omega, \boldsymbol{k}) \;\Rightarrow$$

where $B(\boldsymbol{k})$ is a function of the momentum which has no special peak at the Fermi energy. Since the product $G^{\mathrm{R}}G^{\mathrm{A}}$ has a strong maximum at the Fermi energy one uses the approximation

$$\Rightarrow N_+(\epsilon_{\mathrm{F}}) \int \frac{\mathrm{d}\Omega_k}{S_z} B(k_{\mathrm{F}}, \hat{k}) \int \mathrm{d}\eta\, G^{\mathrm{R}}(\epsilon, \boldsymbol{k})\, G^{\mathrm{A}}(\epsilon - \hbar\omega, \boldsymbol{k}) .$$

$N_+(\epsilon_{\mathrm{F}})$ is the density of one spin state at the Fermi surface, i.e. half the total density of states, $S_z$ is the surface of the unit sphere in $z$ dimensions. The latter integral yields:

$$\int \mathrm{d}\eta\, G^{\mathrm{R}}(\epsilon, \boldsymbol{k})\, G^{\mathrm{A}}(\epsilon - \hbar\omega, \boldsymbol{k}) = \int \mathrm{d}\eta\, \frac{1}{\eta - \epsilon - (\mathrm{i}\hbar/2\tau)} \frac{1}{\eta - \epsilon + \hbar\omega + (\mathrm{i}\hbar/2\tau)} = \frac{2\pi}{1 - \mathrm{i}\omega\tau} \frac{\tau}{\hbar} . \tag{3.4}$$

Finally we obtain:

$$\sigma_{ij}^{(\mathrm{I})}(\omega) = \frac{e^2 v_F^2 N(e_F) \tau}{1 - i\omega\tau} \frac{\delta_{ij}}{z} \tag{3.5}$$

where we have used:

$$\int d\epsilon \frac{f(\epsilon - \hbar\omega) - f(\epsilon)}{\hbar\omega} = 1$$

and:

$$\int \frac{d\Omega_k}{S_z} v_i(k)\, v_j(k) = \delta_{ij} \frac{1}{z} v_F^2 .$$

The factor 2 due to the spin summation is absorbed in $N(\epsilon_F)$. It is easy to show that eq. (3.5) is equivalent to the relation of conductance:

$$\sigma_{ij}^{(\mathrm{I})} = \delta_{ij} \frac{ne^2\tau/m}{1 - i\omega\tau} .$$

In the case of isotropic s-scattering eq. (3.5) yields the leading term in the conductance. For non-isotropic scattering one has to include the so-called ladder diagram of the second electron–hole propagator.

The contribution of the second electron–hole diagram in fig. 3.1 to the conductivity is given by the following expression:

$$\sigma_{ij}^{(\mathrm{II})}(\omega) = e^2 \int \frac{d\epsilon}{2\pi} \frac{f(\epsilon - \hbar\omega) - f(\epsilon)}{\omega} \int \frac{d^z k}{(2\pi)^z} \int \frac{d^z k'}{(2\pi)^z} \sum_{\sigma,\sigma'} v_i(k)\, v_j(k')$$
$$* G_\sigma^{\mathrm{R}}(\epsilon, k)\, G_\sigma^{\mathrm{A}}(\epsilon - \hbar\omega, k)\, \Gamma_{\sigma,\sigma'}(k, k'; \epsilon, \omega)\, G_{\sigma'}^{\mathrm{R}}(\epsilon, k')\, G_{\sigma'}^{\mathrm{A}}(\epsilon - \hbar\omega, k') . \tag{3.6}$$

In the standard case one approximates $\Gamma$ by the sum of ladder diagrams as shown in fig. 3.2.

(A full dot separating two propagator lines represents a scattering by the impurity and a change of momentum. The change of momentum is the same for every two dots which are connected by a dashed line.)

The evaluation which shall not be performed here yields a replacement of $\tau$ in eq. (3.5) by $\tau_{tr}$, the transport lifetime of the conduction electrons. We are going to evaluate $\sigma_{ij}^{(\mathrm{II})}$ for the maximal crossed diagrams which were originally introduced by Langer and Neal [156].

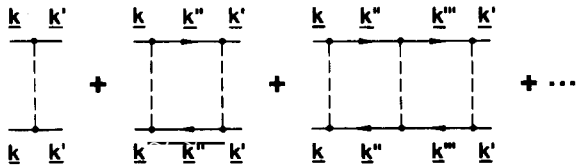


Fig. 3.2. The electron–hole ladder diagram.

### 3.2. Quantum corrections

The following description and derivation of the theoretical results is essentially based on the work by Altshuler et al. [12], Maekawa and Fukuyama [24] and Hikami et al. [7]. As we discussed in section 2 Langer and Neal first studied a particular group of electron–hole propagators, the so-called maximal crossed diagrams which are shown in fig. 3.3.

The value of this group of electron–hole propagators we now denote by $\Gamma(\boldsymbol{k}, \boldsymbol{k}'; \epsilon, \omega)$. We will show below that $\Gamma$ depends only on $\boldsymbol{k} + \boldsymbol{k}' = \boldsymbol{q}$ and $\omega$ and diverges for $|q|$, $\omega \to 0$, but has no structure at $k_F$. Therefore we change the variables from $\boldsymbol{k}, \boldsymbol{k}'$ to $\boldsymbol{k}, \boldsymbol{q}$ ($\int d^z k\, d^z k' \to \int d^z k\, d^z q$). Then $\Gamma$ can be replaced by $\Gamma(\boldsymbol{q}; \omega)$ and the $\eta$ integration can be performed. In the Green's functions of $\boldsymbol{k}'$ one can replace $\boldsymbol{k}'$ by $-\boldsymbol{k} + \boldsymbol{q}$ and therefore $\eta'$ by

$$\eta' = \frac{\hbar^2 k'^2}{2m} = \frac{\hbar^2}{2m}(-\boldsymbol{k} + \boldsymbol{q})^2 \approx \eta - \hbar\, \boldsymbol{v}_F(\boldsymbol{k}) * \boldsymbol{q}\,.$$

Therefore

$$\int \frac{d^z k}{(2\pi)^z} G^R_\sigma(\epsilon, \boldsymbol{k})\, G^A_\sigma(\epsilon - \hbar\omega, \boldsymbol{k})\, G^R_{\sigma'}(\epsilon, -\boldsymbol{k} + \boldsymbol{q})\, G^A_{\sigma'}(\epsilon - \hbar\omega, -\boldsymbol{k} + \boldsymbol{q})$$

$$= N(\epsilon_F) \int_{-\infty}^{+\infty} d\eta \frac{1}{\eta - \epsilon - (i\hbar/2\tau)} \frac{1}{\eta - \epsilon + \hbar\omega + (i\hbar/2\tau)} \frac{1}{(\eta - \hbar\, \boldsymbol{v}_F \boldsymbol{q}) - \epsilon - (i\hbar/2\tau)}$$

$$\times \frac{1}{(\eta - \hbar\, \boldsymbol{v}_F \boldsymbol{q}) - \epsilon + \hbar\omega + (i\hbar/2\tau)}\,.$$

We close the integration path in the upper plane and find two residua:

$$\eta = \epsilon + \frac{i\hbar}{2\tau} \quad \text{and} \quad \eta = \epsilon + \frac{i\hbar}{2\tau} + \hbar\, \boldsymbol{v}_F * \boldsymbol{q}\,,$$

$$= 2\pi i\, N(\epsilon_F) \frac{1}{\hbar\omega + i\hbar/\tau} \frac{1}{\hbar\, \boldsymbol{v}_F \boldsymbol{q}} \frac{(-2)\hbar\, \boldsymbol{v}_F \boldsymbol{q}}{(\hbar\omega + i\hbar/\tau)^2 - (\hbar\, \boldsymbol{v}_F \boldsymbol{q})^2}\,.$$

For small $|q|$ this yields approximately,

$$\approx 4\pi N(\epsilon_F) \left(\frac{\tau}{\hbar}\right)^3 \frac{1}{(1 - i\omega\tau)^3} \approx 4\pi N(\epsilon_F) \left(\frac{\tau}{\hbar}\right)^3$$

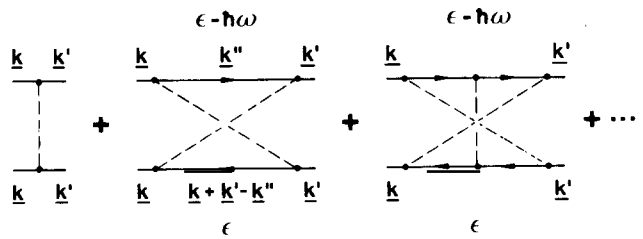


Fig. 3.3. The fan diagram or maximal crossed diagram.

since we are only interested in the low frequency limit. The conductance tensor is diagonal $\sigma_{ij}(\omega) = \delta_{ij}\sigma(\omega)$. We obtain

$$\sigma(\omega)_{\omega\to 0} = -\frac{2\pi N(\epsilon_F)\tau}{\hbar}\frac{e^2}{\pi\hbar}D\tau \sum_{\sigma,\sigma'}\int \frac{d^z q}{(2\pi)^z}\Gamma(q,\omega) \tag{3.7}$$

where we have introduced the diffusion constant:

$$D = \frac{1}{z}v_F^2\tau .$$

Now we calculate $\Gamma(q;\omega)$. First we express one of the electron–hole propagators by the product of the Green's functions and the matrix elements. We take the third diagram in fig. 3.3 and obtain:

$$\sum_{g_1}\sum_{g_2} V_{g_1} G^R(\epsilon, k+g_1)\, V_{g_2} G^R(\epsilon, k+g_1+g_2)\, V_{g_3}$$
$$* V^*_{g_1} G^A(\epsilon-\hbar\omega, k'-g_1)\, V^*_{g_2} G^A(\epsilon-\hbar\omega, k'-g_1-g_2)\, V^*_{g_3} . \tag{3.8}$$

For simplicity one generally assumes isotropic scattering, i.e.

$$|V_{g_1}|^2 = |V_{g_2}|^2 = \frac{1}{2\pi N(\epsilon_F)}\frac{\hbar}{\tau} = \Gamma_0 .$$

Further we define:

$$\Pi(k+k';\epsilon,\omega) = \sum_g G^R(\epsilon, k+g)\, G^A(\epsilon-\hbar\omega, k'-g) . \tag{3.9}$$

It only depends on the sum of $k$ and $k'$ and will be calculated below. Now we can write the considered propagator as:

$$\Gamma_0\Pi(k+k')\Gamma_0\Pi(k+k')\Gamma_0 .$$

Therefore the sum of all maximal crossed diagrams is given by:

$$\Gamma = \Gamma_0 + \Gamma_0\Pi\Gamma_0 + \Gamma_0\Pi\Gamma_0\Pi\Gamma_0 + \cdots = \frac{\Gamma_0}{1-\Gamma_0\Pi} . \tag{3.10}$$

The rearrangement of the Green's functions and matrix elements in eq. (3.8) is generally expressed by a two-particle propagator which means that the upper hole-line is turned around (see fig. 3.4).

Equation (3.10) can be written as a Dyson equation for the two-particle propagator as shown in fig. 3.5.

It is equivalent to the following equation

$$\Gamma(k+k';\omega) = \Gamma_0 + \Gamma_0\Pi(k+k';\omega)\Gamma(k+k';\omega) . \tag{3.11}$$

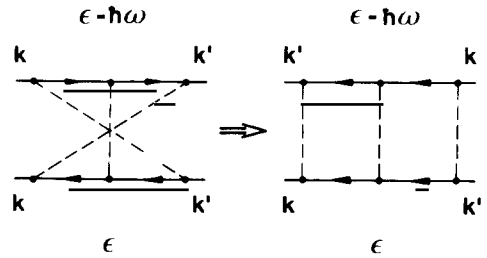


Fig. 3.4. The equivalence of the fan diagram for particle–hole propagators and the ladder diagram for particle–particle propagators.

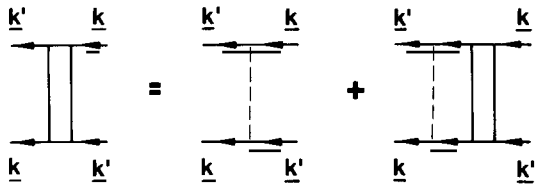


Fig. 3.5. Dyson equation for particle–particle propagators.

We evaluate $\Pi(\boldsymbol{k}+\boldsymbol{k}';\omega)$:

$$\Pi = \int \frac{\mathrm{d}^z g}{(2\pi)^z} G^{\mathrm{R}}(\epsilon, \boldsymbol{k}+\boldsymbol{g})\, G^{\mathrm{A}}(\epsilon-\hbar\omega, \boldsymbol{k}'-\boldsymbol{g}) \Rightarrow$$

We set $\boldsymbol{k}'' = \boldsymbol{k}+\boldsymbol{g}$ and $\boldsymbol{k}+\boldsymbol{k}' = \boldsymbol{q}$,

$$\Rightarrow \int \frac{\mathrm{d}^z k''}{(2\pi)^z} G^{\mathrm{R}}(\epsilon, \boldsymbol{k}'')\, G^{\mathrm{A}}(\epsilon-\hbar\omega, -\boldsymbol{k}''+\boldsymbol{q}) \Rightarrow$$

We expand $\eta_{\boldsymbol{k}''+\boldsymbol{q}}$ for small $|q|$. (The justification that $|q|$ must be small follows below.) Then we obtain:

$$\begin{aligned}
&\Rightarrow N(\epsilon_{\mathrm{F}}) \int \frac{\mathrm{d}\Omega_{k''}}{S_z} \int \mathrm{d}\eta'' \frac{1}{\eta''-\epsilon-(\mathrm{i}\hbar/2\tau)} \frac{1}{\eta''-\epsilon+\hbar\omega-\hbar\, v_{\mathrm{F}} q+(\mathrm{i}\hbar/2\tau)} \\
&= \frac{1}{\hbar} 2\pi\mathrm{i}\, N(\epsilon_{\mathrm{F}}) \int \frac{\mathrm{d}\Omega_{k''}}{S_z} \frac{1}{\omega - v_{\mathrm{F}} q + \mathrm{i}/\tau} \\
&\approx \frac{2\pi N(\epsilon_{\mathrm{F}})}{\hbar} \tau \int \frac{\mathrm{d}\Omega_{k''}}{S_z} [1 + \mathrm{i}\omega\tau - \mathrm{i}\, v_{\mathrm{F}} q\tau + \mathrm{i}^2 (v_{\mathrm{F}} q)^2 \tau^2 - \cdots] \\
&\approx \frac{2\pi N(\epsilon_{\mathrm{F}})}{\hbar} \tau [1 + \mathrm{i}\omega\tau - Dq^2\tau]
\end{aligned} \tag{3.12}$$

where $D = (v_{\mathrm{F}}^2\tau)/z$ is the diffusion constant in $z$ dimensions. Finally we obtain for $\Gamma$:

$$\begin{aligned}
\Gamma(\boldsymbol{k}+\boldsymbol{k}';\omega) &= \frac{\{1/2\pi N(\epsilon_{\mathrm{F}})\}\, \hbar/\tau}{1 - \{1/2\pi N(\epsilon_{\mathrm{F}})\}\, (\hbar/\tau) \{2\pi N(\epsilon_{\mathrm{F}})/\hbar\}\, \tau [1 + \mathrm{i}\omega\tau - D(\boldsymbol{k}+\boldsymbol{k}')^2\tau]} \\
&= \frac{\hbar}{2\pi N(\epsilon_{\mathrm{F}})\, \tau\, D(\boldsymbol{k}+\boldsymbol{k}')^2\, \tau - \mathrm{i}\omega\tau}.
\end{aligned} \tag{3.13}$$

Obviously $\Gamma$ is divergent for $\omega \to 0$ and $\boldsymbol{k}+\boldsymbol{k}' \to 0$ showing a diffusion pole. It justifies the expansion for small $|q|$. So we finally obtain for the corrections in the conductance:

$$\sigma(\omega) = -\frac{e^2}{\pi\hbar} D\tau\, 2 \int \frac{\mathrm{d}^z q}{(2\pi)^z} \frac{1}{Dq^2\tau - \mathrm{i}\omega\tau}. \tag{3.14}$$

Since the main contribution of the integral arises from small $q$-values the $q$-integration might feel the finite dimension of the metal while the original $k$-integration is insensitive. If we have for example a thin film with a thickness $d$ and a mean free path $l$ which is less than $d$ then the first $k$-integration is essentially a three-dimensional integration. However, for the $q$-integration the allowed $q$-states are planes perpendicular to $q_z$ with $q_z$ equal to $\nu\pi/d$ ($\nu = 0, 1, 2, \ldots$). Therefore we introduced a different dimensionality $z'$ for the $q$-integration. Here we are interested in the two-dimensional case of weak localization and set $z' = 2$. (It is important to keep in mind that the diffusion constant contains the dimensionality $z$ of the original $k$-integration.) For $z' = 2$ we obtain for the quantum corrections of the conductivity:

$$\Rightarrow \sigma(\omega) = -2\frac{e^2}{\pi\hbar} D\tau \frac{1}{(2\pi)^2} \int_0^{(D\tau)^{-1/2}} \pi \, dq^2 \frac{1}{D\tau q^2 - i\omega\tau} \Rightarrow \tag{3.14a}$$

The upper limit of the integration is a cut-off. It corresponds to the shortest diffusion step in space which is the diffusion during one single collision time. (The exact value of the upper limit has no influence on the final result.) As we saw in the preceding section we obtain for the dc conductivity of the quantum corrections a damping due to inelastic scattering. This damping results in replacing $(-i\omega)$ by $1/\tau_i$. So we obtain:

$$\Rightarrow \sigma(0) = -\frac{e^2}{2\pi^2\hbar} \ln\left(\frac{\tau_i}{\tau}\right). \tag{3.14b}$$

*3.3. Connection with the physical interpretation*

We want to justify the replacement of $(-i\omega)$ by $1/\tau_i$. In addition the width of the back-scattering spot which we introduced in section 2 will be derived. For this purpose we apply at the time $t = 0$ an electric field of $\delta$-form,

$$E(t) = \delta(t) E_0 = E_0 \int_{-\infty}^{+\infty} \frac{d\omega}{2\pi} \exp(-i\omega t).$$

The response to this electric field can be calculated with the conductivity in eq. (3.14a). The resulting current is $j(\omega) = \sigma(\omega) * E(\omega)$. Therefore the time dependence of the current is given by

$$j(t) = -\frac{2e^2}{\pi\hbar} D\tau \frac{1}{(2\pi)^2} \int \frac{d\omega}{2\pi} \int d^2q \frac{1}{D\tau q^2 - i\omega\tau} \exp(-i\omega t) E_0$$

We perform the $\omega$-integration:

$$= -\frac{2e^2}{\pi\hbar} D \frac{1}{(2\pi)^2} \int d^2q \exp(-Dq^2 t) E_0. \tag{3.14c}$$

This result demonstrates that essentially only such $q$-values contribute to the current for which $Dq^2 t$

is less than 1 which means that the radius of the spot around $(-\boldsymbol{k})$ is roughly given by $q_c^2 = 1/(Dt)$. Larger values of $|q|$ are suppressed by the Gauss distribution. Furthermore we see that a peaked electric field causes a slowly decaying current in opposite direction which is identical with the "echo" we discussed above. Although the inelastic processes are not included in this calculation one realizes that they cause an additional exponential decay proportional to $\exp(-t/\tau_i)$ because the coherence decays with this characteristic time. If we multiply (3.14c) by $\exp(-t/\tau_i)$ and return to the $\omega$ representation we find:

$$\sigma(\omega) = -2\frac{e^2}{\pi\hbar} D\tau \frac{1}{(2\pi)^2} \int \mathrm{d}^2 q \, \frac{1}{D\tau q^2 + \tau/\tau_i - \mathrm{i}\omega\tau}. \tag{3.15}$$

Now we easily obtain the dc conductivity by setting $\omega = 0$. In the following the general procedure will be to neglect the inelastic processes during the calculation and to replace $(-\mathrm{i}\omega)$ by $1/\tau_i$ in the final result.

### 3.4. *Magnetic field*

An external magnetic field perpendicular to the two-dimensional film plane has a strong influence on the quantum interference. The vector potential which is caused by the magnetic field modifies the phase of the wave functions which results in a partial destruction of the quantum interference. We consider a two-dimensional system in which the mean free path is much smaller than the cyclotron radius. Then the main effect of the vector potential on the electronic wave function or on the Green's function respectively is a change of the phase between two different points. If $G(\boldsymbol{r} - \boldsymbol{r}')$ is the Green's function in the absence of an external magnetic field then in the presence of a magnetic field (or a vector potential respectively) it is given by:

$$\tilde{G}(\boldsymbol{r}, \boldsymbol{r}') = G(\boldsymbol{r} - \boldsymbol{r}') \exp\left[\frac{\mathrm{i}e}{\hbar} \int_{\boldsymbol{r}}^{\boldsymbol{r}'} \boldsymbol{A}(\boldsymbol{s})\,\mathrm{d}\boldsymbol{s}\right]. \tag{3.16}$$

In the presence of a vector potential the Green's function is no longer translational invariant. With these modified Green's functions we can repeat the earlier summation of the crossed diagrams. However, now it is favourable to perform the calculation in real space instead of momentum space. Then one obtains:

$$\begin{aligned}\tilde{\Pi}(\boldsymbol{r}, \boldsymbol{r}_1; \omega) &= \widetilde{G^{\mathrm{A}}}(\boldsymbol{r}, \boldsymbol{r}_1; \epsilon - \hbar\omega)\, \widetilde{G^{\mathrm{R}}}(\boldsymbol{r}, \boldsymbol{r}_1; \epsilon) \\ &= G^{\mathrm{A}}(\boldsymbol{r} - \boldsymbol{r}_1; \epsilon - \hbar\omega)\, G^{\mathrm{R}}(\boldsymbol{r} - \boldsymbol{r}_1; \epsilon) \exp\left[\frac{2\mathrm{i}e}{\hbar} \int_{\boldsymbol{r}}^{\boldsymbol{r}_1} \boldsymbol{A}(\boldsymbol{s})\,\mathrm{d}\boldsymbol{s}\right] \\ &= \Pi(\boldsymbol{r} - \boldsymbol{r}_1; \omega) \exp\left[\frac{2\mathrm{i}e}{\hbar} \int_{\boldsymbol{r}}^{\boldsymbol{r}_1} \boldsymbol{A}(\boldsymbol{s})\,\mathrm{d}\boldsymbol{s}\right].\end{aligned} \tag{3.17}$$

Now we want to demonstrate that this is equivalent to the replacement of $\boldsymbol{q}$ by $\boldsymbol{q} + 2e\boldsymbol{A}/\hbar$ in $\Pi(\boldsymbol{q}; \epsilon, \omega)$. For this purpose Altshuler et al. considered $\Pi(\boldsymbol{r}, \boldsymbol{r}'; \omega)$ as an operator with its eigenfunctions $\psi_\eta(\boldsymbol{r})$ so

that:

$$\int \tilde{\Pi}(\boldsymbol{r}, \boldsymbol{r}'; \omega)\, \psi_\eta(\boldsymbol{r}')\, \mathrm{d}^3\boldsymbol{r}' = \lambda(\eta)\, \psi_\eta(\boldsymbol{r})\,. \tag{3.18}$$

Introducing the vector potential one obtains:

$$\int \Pi(\boldsymbol{r}-\boldsymbol{r}'; \omega) \exp\left[\frac{2\mathrm{i}e}{\hbar}\int_{\boldsymbol{r}}^{\boldsymbol{r}'} \boldsymbol{A}(\boldsymbol{s})\,\mathrm{d}\boldsymbol{s}\right] \psi_\eta(\boldsymbol{r}')\,\mathrm{d}^3\boldsymbol{r}' = \lambda(\eta)\,\psi_\eta(\boldsymbol{r})\,.$$

We expand $\boldsymbol{A}(\boldsymbol{s})$ and $\psi_\eta(\boldsymbol{r}')$ about $\boldsymbol{r}$ up to second order and obtain:

$$\left[\Pi(\boldsymbol{q}=0;\omega) + \frac{1}{2}\frac{\partial^2\Pi(q=0;\omega)}{\partial q^2}\left(\frac{\nabla}{\mathrm{i}} + \frac{2e}{\hbar}\boldsymbol{A}\right)^2\right]\psi_\eta(\boldsymbol{r}) = \lambda(\eta)\,\psi_\eta(\boldsymbol{r})\,. \tag{3.19}$$

Here it was used that:

$$\int \Pi(\boldsymbol{r}-\boldsymbol{r}';\omega)\,(\boldsymbol{r}-\boldsymbol{r}')^2\,\mathrm{d}^3\boldsymbol{r}' = -\frac{\partial^2}{\partial \boldsymbol{q}^2}\Pi(\boldsymbol{q};\omega)\Big|_{q=0}\,.$$

Eq. (3.19) demonstrates that the eigenfunctions of $\Pi(\boldsymbol{r}, \boldsymbol{r}'; \omega)$ are identical with the wave functions of particles of charge $2e$ in a magnetic field. One further realizes that in a magnetic field $\boldsymbol{q} = \boldsymbol{k} + \boldsymbol{k}'$ can be replaced by $\boldsymbol{q} + 2e\boldsymbol{A}/\hbar$. Here $\boldsymbol{q}$ corresponds to a momentum of the doubly charged particle. In a magnetic field $(\boldsymbol{q} + 2e\boldsymbol{A}/\hbar)^2$ is quantized. This leads to the replacement rule

$$q^2 \Rightarrow q_n^2 = \frac{4eH}{\hbar}\left(n + \frac{1}{2}\right). \tag{3.20}$$

With the above calculated value of $\Pi$, eq. (3.12), the eigenvalue of $\lambda$ in a magnetic field is given by:

$$\lambda_n = \frac{2\pi N(\epsilon_\mathrm{F})}{\hbar}\tau\left[1 + \mathrm{i}\omega\tau - D\tau\frac{4eH}{\hbar}\left(n+\frac{1}{2}\right)\right]. \tag{3.21}$$

We may calculate $\tilde{\Pi}(\boldsymbol{r}, \boldsymbol{r}'; \omega)$ by multiplying eq. (3.18) by $\psi_\eta^*(\boldsymbol{r}'')$ and summing over all $\eta$. This yields:

$$\int \tilde{\Pi}(\boldsymbol{r}, \boldsymbol{r}'; \omega) \sum_\eta \psi_\eta^*(\boldsymbol{r}'')\,\psi_\eta(\boldsymbol{r}')\,\mathrm{d}^3\boldsymbol{r}' = \sum_\eta \lambda(\eta)\,\psi_\eta^*(\boldsymbol{r}'')\,\psi_\eta(\boldsymbol{r})$$

$$\tilde{\Pi}(\boldsymbol{r}, \boldsymbol{r}''; \omega) = \frac{2H}{\pi\hbar}\sum_n \psi_n(\boldsymbol{r})\,\psi_n^*(\boldsymbol{r}'')\,\lambda_n\,. \tag{3.22}$$

The pre-factor of the sum takes care of the degeneracy of the quantized state (for one spin orientation). Since the $\tilde{\Pi}(\boldsymbol{r}, \boldsymbol{r}'; \omega)$ depends on the variables of real space $\boldsymbol{r}$ and $\boldsymbol{r}'$ one may proceed in calculating also $\Gamma$ in real space and use the Kubo formula in real space to calculate finally the conductivity. We can, however, use the above calculation for $\Gamma(q; \omega)$ and $\sigma(\omega)$ to obtain the corresponding functions $\Gamma(q; \omega)$

and $\sigma(\omega)$ in a magnetic field. The only change is the quantization of $q^2$. Therefore we find:

$$\Gamma(q_n;\omega)=\frac{\hbar}{2\pi N(\epsilon_F)\tau}\,\frac{1}{D\tau q_n^2-i\omega\tau}. \tag{3.23}$$

The corresponding equation to (3.14a) for the conductivity is:

$$\sigma(\omega=0,H)=-2\frac{e^2}{\pi\hbar}D\tau\frac{eH}{\pi\hbar}\sum_{n=0}^{\hbar/D\tau 4eH}\frac{1}{D\tau(4eH/\hbar)(n+\frac{1}{2})+\tau/\tau_i}. \tag{3.24a}$$

For the dc conductivity we replaced $(-i\omega)$ by $1/\tau_i$. The sum over $n$ can be expressed in terms of two digamma functions,

$$\sigma(\omega=0,H)=-\frac{e^2}{2\pi^2\hbar}\left[\Psi\left(\frac{1}{2}+\frac{\hbar}{4eDH\tau}\right)-\Psi\left(\frac{1}{2}+\frac{\hbar}{4eDH\tau_i}\right)\right]. \tag{3.24b}$$

The first digamma function can be approximated by $\ln(\hbar/4eDH\tau)$, its asymptotic limit for large argument.

### *3.5. Spin–orbit scattering and magnetic scattering*

Until now we discussed only scattering processes where the spin of the electron was conserved. This is no longer correct if one includes spin–orbit scattering and scattering by magnetic impurities. Let us first consider spin–orbit scattering. If an electron with spin $\sigma$ is scattered by a Coulomb potential $V(r)$ from the state $\boldsymbol{k}$ into the state $\boldsymbol{k}'$ the matrix element of the scattering is given by:

$$V_{k-k'}[1+ic(\boldsymbol{k}\times\boldsymbol{k}')\boldsymbol{\sigma}] \tag{3.25}$$

where $c$ is a small constant. In analogy to eq. (3.8) we form the product of the corresponding matrix elements. We obtain instead of $\Gamma_0=\overline{V_{k,k'}V^*_{k,k'}}$:

$$\Gamma^0_{\alpha\beta,\gamma\delta}=\frac{\hbar}{2\pi N(\epsilon_F)}\left[\frac{1}{\tau_0}\delta_{\alpha\beta}\,\delta_{\gamma\delta}-\sum_i\frac{1}{\tau^i_{so}}\sigma^i_{\alpha\beta}\sigma^i_{\gamma\delta}\right]. \tag{3.26}$$

In analogy to the replacement of $|V_g|^2$ by $[2\pi N(\epsilon_F)\tau_0/\hbar]^{-1}$ we have to replace the second term $|V_g|^2c^2(\boldsymbol{k}\times\boldsymbol{k}')_i^2$ by $[2\pi N(\epsilon_F)\tau^i_{so}/\hbar]^{-1}$. In the two-particle operator $\Gamma$ we now have to include the spins of the electron lines.

The new Dyson equation in analogy to fig. 3.5 and eq. (3.11) is shown in fig. 3.6.
This corresponds to the equation

$$\Gamma_{\alpha\beta,\gamma\delta}=\Gamma^0_{\alpha\beta,\gamma\delta}+\sum_{\mu,\nu}\Gamma^0_{\alpha\mu,\gamma\nu}\,\Pi_{\mu\nu}\,\Gamma_{\mu\beta,\nu\delta}\,. \tag{3.27}$$

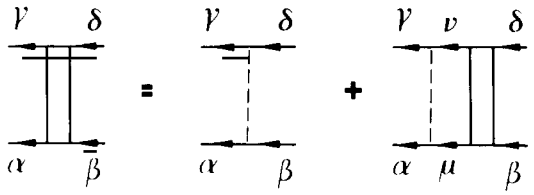


Fig. 3.6. Dyson equation for particle–particle propagators in the presence of spin–orbit scattering.

This yields for isotropic spin–orbit scattering:

$$\Gamma^0_{++,++} = \Gamma^0_{--,--} = \frac{\hbar}{2\pi N(\epsilon_F)} * \left(\frac{1}{\tau_0} - \frac{1}{3}\frac{1}{\tau_{so}}\right)$$

$$\Gamma^0_{+-,-+} = \Gamma^0_{-+,+-} = -\frac{\hbar}{2\pi N(\epsilon_F)}\frac{2}{3}\frac{1}{\tau_{so}} \tag{3.28}$$

$$\Gamma^0_{++,--} = \Gamma^0_{--,++} = \frac{\hbar}{2\pi N(\epsilon_F)} * \left(\frac{1}{\tau_0} + \frac{1}{3}\frac{1}{\tau_{so}}\right).$$

All other $\Gamma^0$ vanish.

In the evaluation of the conductivity in the Kubo formula [eq. (3.6)] one has to pay attention that on the one hand the spin of the entering electron and hole must be identical and on the other hand the spin of the leaving electron and hole. This means that only those $\Gamma$ contribute to the conductivity with $\alpha = \delta$ and $\beta = \gamma$. Therefore the quantum correction to the conductivity is in analogy to eq. (3.7):

$$\sigma(\omega) = -\frac{2\pi N(\epsilon_F)\tau}{\hbar}\frac{e^2}{\pi\hbar} D\tau \int \frac{d^2q}{(2\pi)^2} (\Gamma_{++,++} + \Gamma_{--,--} + \Gamma_{+-,-+} + \Gamma_{-+,+-}). \tag{3.29}$$

In a perpendicular magnetic field one has to replace, as we saw above, $\int d^2q/(2\pi)^2$ by $eH/\pi\hbar \sum_n$. The influence of the magnetic field on the magnetic moment of the electrons, i.e. the Zeeman term, is neglected in the evaluation. It has been calculated by Maekawa and Fukujama [24] but it turned out that its influence can be neglected for thin films with a mean free path down to 10 Å. Therefore $\Pi(\boldsymbol{k}+\boldsymbol{k}';\omega)$ is not modified and given by eq. (3.12). The relaxation time $\tau$ which appears in the denominator of the Green's functions is given by:

$$\tau^{-1} = \tau_0^{-1} + \tau_{so}^{-1}. \tag{3.30}$$

(In the presence of magnetic scattering one has an additional term $\tau_s^{-1}$ on the right side.)

One may expect that the small contribution of $1/\tau_{so}$ to $1/\tau_0$ could be neglected. This is, however, not the case because one finds a cancellation of the in- and out-going scattering processes in the denominator of eq. (3.10) and even small contributions as $1/\tau_{so}$ destroy the divergence of this denominator. We obtain from the

Dyson equation (3.27)

$$\Gamma_{++,++} = \Gamma_{--,--} = \frac{\Gamma^0_{++,++}}{1 - \Gamma^0_{++,++}\Pi} = \frac{\hbar}{2\pi N(\epsilon_F)\tau} \frac{1}{Dq^2\tau - i\omega\tau + \frac{4}{3}\tau/\tau_{so}} \tag{3.31a}$$

and:

$$\Gamma_{+-,-+} = \Gamma_{-+,+-} = \frac{\Gamma^0_{+-,-+}(1 - \Gamma^0_{++,--}\Pi) + \Gamma^0_{++,--}\Gamma^0_{+-,-+}\Pi}{|1 - \Gamma^0_{++,--}\Pi|^2 - |\Pi|^2(\Gamma^0_{+-,-+})^2} = \frac{\hbar}{4\pi N(\epsilon_F)\tau}\left(\frac{1}{Dq^2\tau - i\omega\tau + \frac{4}{3}\tau/\tau_{so}} - \frac{1}{Dq^2\tau - i\omega\tau}\right)\frac{2}{3}\frac{\tau}{\tau_{so}}. \tag{3.31b}$$

We proceed the calculation for finite magnetic field because it includes the case $H = 0$ and obtain for the additional conductivity:

$$\sigma(\omega = 0, H) = -\frac{e^2}{2\pi^2\hbar}\left[\Psi\left(\frac{1}{2} + \frac{H_1}{H}\right) - \Psi\left(\frac{1}{2} + \frac{H_2}{H}\right) + \frac{1}{2}\Psi\left(\frac{1}{2} + \frac{H_3}{H}\right) - \frac{1}{2}\Psi\left(\frac{1}{2} + \frac{H_4}{H}\right)\right] \tag{3.32}$$

where:

$$\begin{aligned} H_1 &= H_o + H_{so} + H_s \\ H_2 &= \tfrac{4}{3}H_{so} + \tfrac{2}{3}H_s + H_i \\ H_3 &= 2H_s + H_i \\ H_4 &= \tfrac{4}{3}H_{so} + \tfrac{2}{3}H_s + H_i . \end{aligned} \tag{3.32a}$$

The characteristic fields $H_n$ are connected with the characteristic relaxation times $\tau_n$ by the relation:

$$H_n\tau_n = \frac{\hbar}{4eD}. \tag{3.33}$$

Here the indices stand for the following scattering processes:

o = potential scattering
i = inelastic scattering
s = magnetic scattering
so = spin–orbit scattering.

The above calculation has been performed for $H_s = 0$, i.e. no magnetic scattering. We have, however, included the effect of a finite magnetic scattering into the final result to avoid additional formulae.

Magnetic scattering is generally due to an exchange interaction between the magnetic impurity and the conduction electron and expressed by a perturbation Hamiltonian of the form $JS\sigma$. The magnetic

impurities cause a magnetic scattering time:

$$\frac{1}{\tau_s^i} = \frac{2\pi N(\epsilon_F)}{\hbar} n_j J^2 \langle S^i \rangle^2 \tag{3.34}$$

where $i$ denotes the component $i$, $n_j$ is the magnetic impurity concentration and $\langle S^i \rangle^2$ is the thermal average of $(S^i)^2$. This yields for $\Gamma_0$

$$\Gamma^0_{\alpha\beta,\gamma\delta} = \frac{\hbar}{2\pi N(\epsilon_F)} \left[ \frac{1}{\tau_0} \delta_{\alpha\beta} \delta_{\gamma\delta} + \sum_i \left( \frac{1}{\tau_s^i} - \frac{1}{\tau_{so}^i} \right) \sigma^i_{\alpha\beta} \sigma^i_{\gamma\delta} \right]. \tag{3.35}$$

Now one can repeat the above calculation with the new $\Gamma_0$ and

$$\tau^{-1} = \tau_0^{-1} + \tau_{so}^{-1} + \tau_s^{-1}$$

and one obtains the result of eqs. (3.32), (3.32a). In most practical cases the relative contribution of the spin–orbit scattering and the magnetic scattering to the elastic lifetime is so small that $\tau$ can be replaced by $\tau_0$ in the final equations.

## 4. General predictions of the theory

Since the theoretical equations are rather complex and do not give a transparent insight into the dependence of the resistance on the various parameters the theoretical features are plotted in figs. 4.1–4 for a few characteristic cases.

Since for weak localization in two-dimensional systems the conductance is the more appropriate quantity because the conductance correction does not directly depend on the resistance, thickness, elastic free path of the electrons etc. and is proportional to the universal conductance $L_{00}$ which depends only on universal constants, it would be reasonable to use $\Delta L/L_{00}$ as the ordinate. On the other hand one is much more familiar with a resistance plot – in particular as a function of the temperature. Therefore we choose for the scale on the left ordinate the resistance (per square) and on the right ordinate in negative direction $L/L_{00}$. For a comparison with the theory only the right scale is relevant.

### *4.1. Temperature dependence*

In fig. 4.1 the resistance (normalized conductance $\Delta L/L_{00}$) is plotted as a function of $\ln(1/\tau_i)$ which is the natural variable in the problem. The heavy full line describes the logarithmic dependence of $\Delta R$ ($\Delta L/L_{00}$) on the inelastic scattering time in the absence of spin–orbit scattering and magnetic scattering. The heavy dashed curve yields the resistance for finite spin–orbit scattering with $\tau_{so} = 1$. The other thin full curves ($1/\tau_{so} = 0$) and thin dashed curves ($1/\tau_{so} = 1$) are calculated for a different strength of the magnetic scattering. The parameter at the curves is $\ln(1/\tau_s)$. (The times are measured in appropriate units in this schematic calculation.) One recognizes that – in the absence of magnetic scattering – the spin–orbit scattering reverses the sign of the slope for $1/\tau_i < 1/\tau_{so}$. Since one expects a non-vanishing spin–orbit scattering in every metal this behaviour should dominate in every thin film at sufficiently low temperature. The fact that such an increase of the conductance has not yet been observed by experiment is

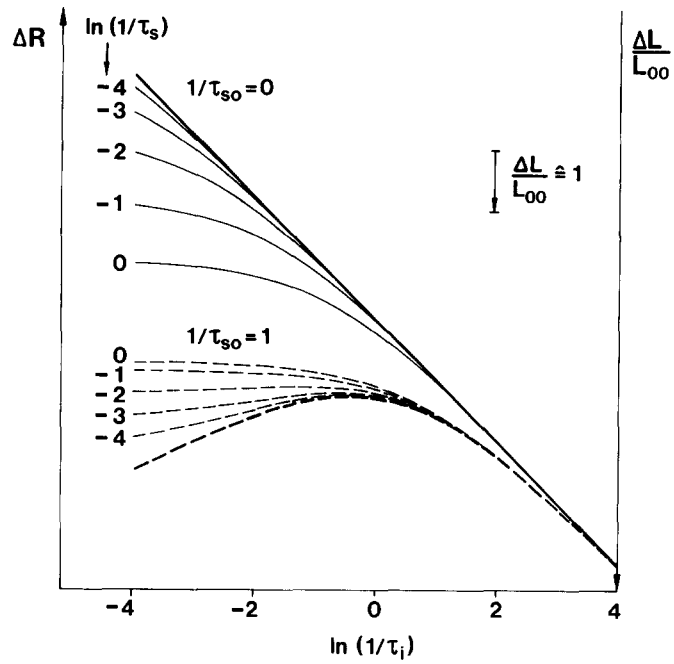


Fig. 4.1. The resistance (normalized conductance $\Delta L/L_{00}$ right scale) plotted as a function of $\ln(1/\tau_i)$. The heavy full line corresponds to $1/\tau_{so} = 0$ and $1/\tau_s = 0$, i.e. no spin–orbit scattering and no magnetic scattering. The thick dashed curve yields the conductance for $\tau_{so} = 1$. The other thin full curves ($1/\tau_{so} = 0$) and thin dashed curves ($1/\tau_{so} = 1$) are calculated for different strength of the magnetic scattering. The parameter at the curves is $\ln(1/\tau_s)$.

due to the additional resistance anomaly caused by the electron–electron interaction. In addition magnetic scattering blocks the influence of quantum interferences for $\tau_i > \tau_s$ as fig. 4.1 demonstrates.

### *4.2. Magneto-resistance*

In fig. 4.2 the resistance is plotted as a function of the applied field. The spin–orbit scattering and the magnetic scattering are set to zero. The third axis is $\ln(H_i)$. (Both $H$ and $H_i$ are measured in the same although arbitrary units.) The width of the magneto-resistance curves is proportional to $H_i$ and $[L(H) - L(0)]/L_{00}$ is a universal function of $H/H_i$. The dashed line (at $H = 0$) yields essentially the linear increase of the resistance as a function of the logarithm of $H_i$ or $1/\tau_i$ respectively.

Fig. 4.3 shows the influence of the spin–orbit scattering. The corresponding magneto-resistance curves are calculated for $H_{so} = 1$. One recognizes that the magneto-resistance reverses its sign for $H_i \ll H_{so}$ at low fields whereas in large fields the negative magneto-resistance behaviour is recovered.

The magneto-resistance curves are for $H_i \ll H_{so}$ almost as narrow as for $H_{so} = 0$. This is demonstrated in fig. 4.4 which shows $\Delta R(H)$ (or $[L(H) - L(0)]/L_{00}$ respectively) for different ratios of $H_{so}/H_i$. The numbers at the curves give this ratio. The figure demonstrates that for small ratios the spin–orbit scattering broadens the magneto-resistance curves. For large spin–orbit scattering ($H_{so} \gg H_i$) and $H \ll H_{so}$ the influence of the spin–orbit scattering is saturated. The magneto-resistance curves show a similar bell shape as for $H_{so} = 0$, however, with opposite sign and only half the amplitude. Therefore a quantitative determination of $H_i$ is possible by saturating the spin–orbit scattering.

The influence of magnetic scattering is quite different and demonstrated in fig. 4.5. Here the spin–orbit scattering is set to zero and the characteristic field $H_s$ for magnetic scattering is set equal to 1.

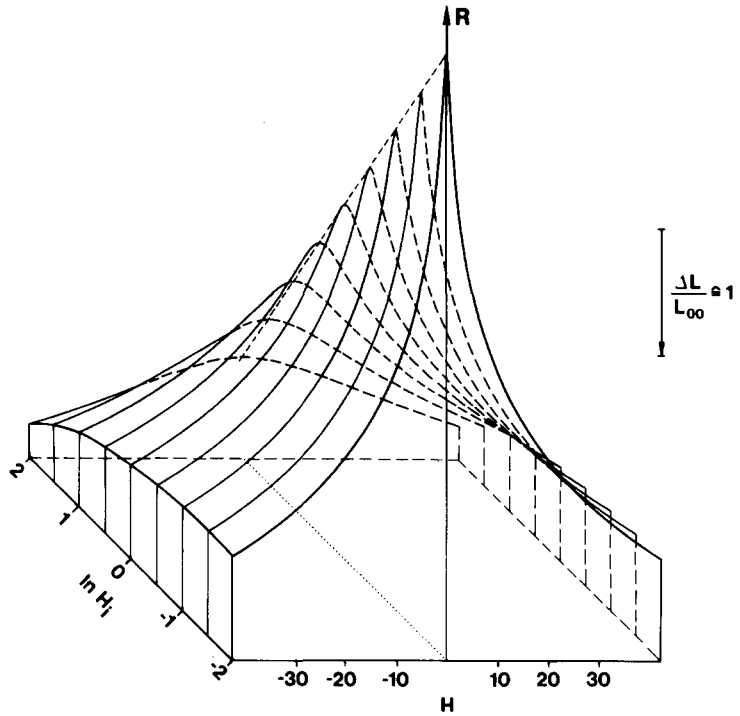


Fig. 4.2. The resistance (normalized conductance $\Delta L/L_{00}$) as a function of the applied magnetic field $H$. $H_{so}$ and $H_s$ are set equal to 0. Parameter is the inelastic field $H_i$. The third axis is $\ln(H_i)$.

As a result the magneto-resistance curves remain broad for $H_i < H_s$. Roughly speaking the effect of a finite $H_s$ is similar to a finite $H_i$. Both corresponding times $\tau_s$ and $\tau_i$ give the upper limit for the coherent interference of the two complementary scattered electron waves.

The magneto-resistance curve of a real thin film is determined by several characteristic times or fields

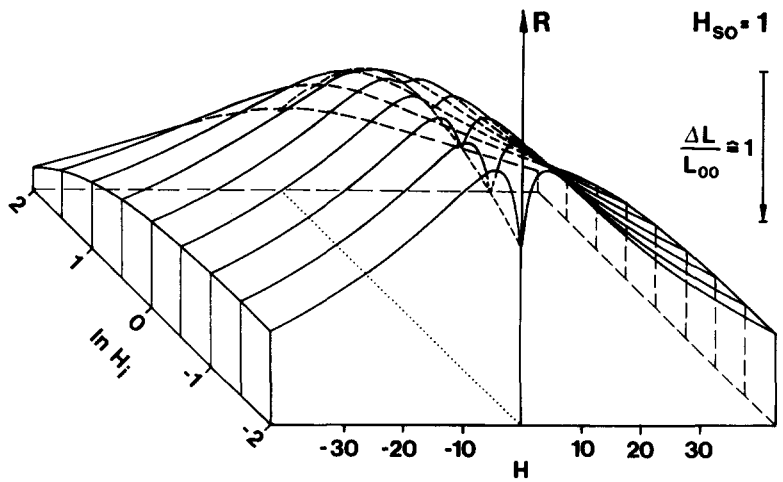


Fig. 4.3. The resistance (normalized conductance $\Delta L/L_{00}$) as a function of the applied magnetic field $H$. $H_{so}$ is set equal to 1 and $H_s = 0$. The third axis gives the parameter $\ln(H_i)$.

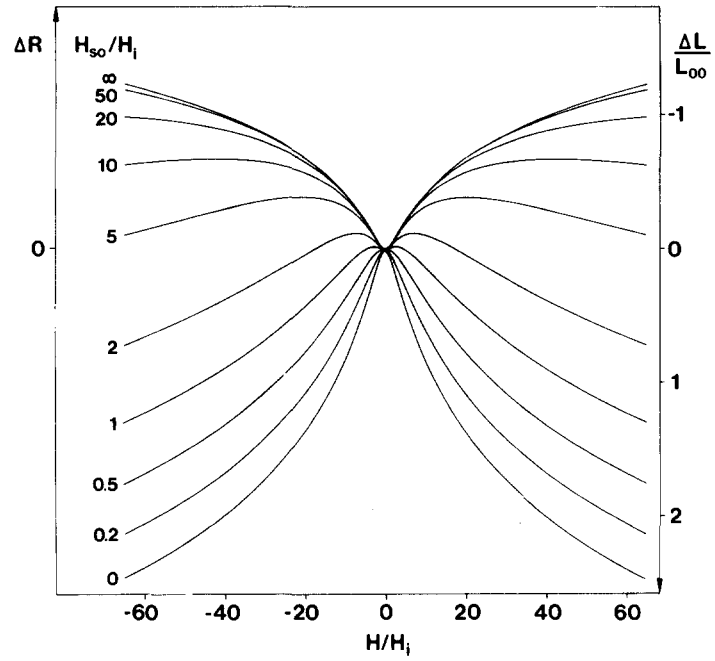


Fig. 4.4. The resistance (normalized conductance $\Delta L/L_{00}$) as a function of the applied field for different ratios of $H_{so}/H_i$.

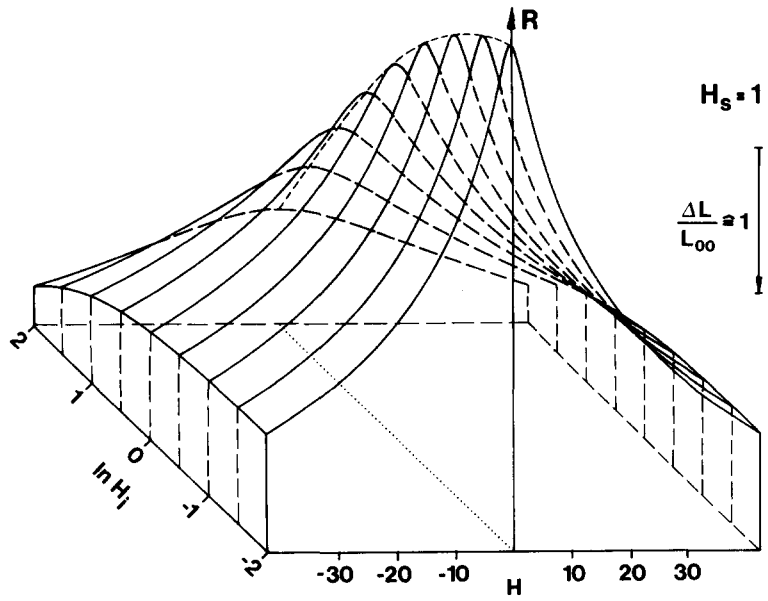


Fig. 4.5. The resistance (normalized conductance $\Delta L/L_{00}$) as a function of the applied magnetic field $H$. $H_s$ is set equal to 1 and $H_{so} = 0$. The third axis gives the parameter $\ln(H_i)$.

respectively, $H_i$, $H_{so}$ and $H_s$. The evaluation is not generally unique. This is demonstrated in [105] where it is shown that the same magneto-resistance curves are obtained for different parameter sets of $H_i$ and $H_{so}$ or $H_i$ and $H_s$ respectively.

## 5. Experimental results

As we discussed before magneto-resistance measurements allow to determine characteristic electronic times in two-dimensional systems. Since it is possible or even probable that the electronic properties and therefore the characteristic times depend on the properties of the metallic films we first want to consider the different methods of film preparation.

### *5.1. Film preparation*

(1) *Room temperature condensation.*

Here the thin films are condensed onto a substrate of room temperature in a high vacuum system or even in an ultra-high vacuum. Since the metal forms first islands during the condensation which need a critical thickness to grow together one has to distinguish two different cases: (a) the film still has a high resistance because there is only a weak contact between the different islands. In this case the film is highly inhomogeneous; one has a very good conductance within each island and a poor conductance between the different islands (may even be a tunnelling contact). It is often argued that the inhomogenity is not relevant for weak localization as long as the Thouless length is larger than the grain size, but I doubt this optimism. (b) When the islands have grown together and form a homogeneous film one finds (for simple and noble metals) generally a rather small defect concentration and therefore rather small resistances. Their electrons are mainly scattered at the surface. Fermi velocity and other electronic properties should be close to the bulk. For inelastic scattering the surface properties may be important and in particular those films which are not protected against air during the transfer from the evaporation system into the cryostate may be influenced by oxidation as well as absorbed impurities at the surface.

(2) *Quenched condensation.*

Here thin films are condensed onto a substrate at helium temperature. Because of the low condensation temperature the metal atoms have a low diffusion mobility. This has two consequences: (i) the critical thickness at which a condensed film becomes continuous is considerably smaller than for room temperature condensation and it is possible to prepare homogeneous films with high resistance; (ii) the physical properties of the highly disordered films differ from the perfect metal. For example if the metal is a superconductor its superconducting transition temperature is enhanced in the quench condensed state because of a change in the electron–phonon interaction and the phonon spectrum.

(3) *Interoxidized film.*

This method has been applied by the Tokyo group [86]. They condense first a film for example Cu with a thickness of 20 Å. This film is not continuous. Then they oxidize the metal which hinders the diffusion. Afterwards the whole procedure is repeated a few times until a film with the required resistance is obtained. One will expect that this $Cu/CuO_x$ differs in some of its properties from pure Cu-films and its inelastic lifetime as well.

(4) *Sputtered films.*

Another rather popular method to prepare films is sputtering. It yields rather homogeneous films with a high degree of disorder. This method has hardly been applied in the investigation of weak localization.

### 5.2. Two-dimensionality

The effect of finite film thickness has been discussed by Altshuler and Aronov [27], Berggren [53] and Ovadyahu et al. [91]. For QUIAD thin disordered films can generally be considered as two-dimensional. However, since a thin film can be two-dimensional for one phenomenon and three-dimensional for another it is useful to discuss the dimension of a thin film more generally including the effect of electron–electron interaction which is treated only in section 7.

One has to distinguish between the dimensionality of different physical situations:

(1) *Normal conductance.*

With respect to the normal conduction process a film is three-dimensional when the thickness $d$ of the film is larger than the mean free path $l$. If the normal conduction process is three-dimensional then one has to use the three-dimensional diffusion constant $D = lv_F/3$ in the former equations.

(2) *Weak localization.*

The thin film is two-dimensional with respect to weak localization when the diffusion time from the top of the film to the bottom is small compared to the characteristic time of the electrons. In zero magnetic field this time is the inelastic lifetime of the conduction electrons. The condition for two-dimensionality is therefore in zero field: $d^2 \ll D\tau_i$. In a finite field the characteristic time is the smaller value of $\tau_i$ and $t_H = \hbar/(4eDH)$. For large fields the corresponding condition is therefore: $d^2 \ll Dt_H = \hbar/(4eH)$.

(3) *Electron–electron interaction.*

For the electron–electron interaction (see section 7) the characteristic time is $\tau_T = \hbar/(2\pi k_B T)$. Therefore a thin film is two-dimensional when $d^2 \ll D\hbar/(2\pi k_B T)$.

(4) *Phonons.*

The dimensionality of the experimental film with respect to the phonons is rather delicate. The most probable phonon wave number at a finite temperature $T$ is roughly $q_T \approx 2k_B T/(\hbar c)$ where $c$ is the sound velocity. Therefore, with respect to the phonons one is often in the intermediate range between two and three dimensions. However, the fact that the thin film is in direct contact to the quartz substrate will enhance the three-dimensionality because the phonons extend into the quartz – despite a mismatch at the interface.

It is, however, not difficult to extend the theoretical formulae of weak localization to a finite film thickness. In the derivation of the correction to the conductance one has to perform a summation over the pseudo-momentum $q$. For a two-dimensional system one sets $q_z = 0$ and neglects all other values of $q_z$. For a finite film thickness one has to add the contribution of finite $q_z$. There are two possibilities to include finite $q_z$ depending on the boundary conditions for the Cooperon. With periodic boundary conditions $q_z$ can take the values $\nu 2\pi/d$, where $\nu$ takes all integers from minus infinity to plus infinity.

Another boundary which is used in superconducting films and which corresponds to vanishing gradient at the surfaces yields $q_z = \nu\pi/d$ where $\nu$ takes all values between zero and plus infinity and appears to be more appropriate. Then one has to replace $q^2$ by $q_{xy}^2 + q_z^2$ and sum over all allowed $q_z$, i.e. all $\nu$. For the magneto-resistance formulae for example one has to replace the argument in the digamma function $[\frac{1}{2} + H_n/H]$ by $[\frac{1}{2} + H_n/H + \nu^2(H_d/H)]$, where $H_d = (\hbar\pi^2)/(4ed^2)$. Afterwards one has to sum over $\nu$ from zero to infinity. In the limit of $d \to \infty$ one recovers the three-dimensional case.

### 5.3. Magneto-resistance measurements

As we discussed above the magneto-resistance is the most reliable method to investigate the quantum interferences at defects. It is hardly affected by the Coulomb anomaly and reflects the interesting electronic times.

The first experimental finding of magneto-resistance in thin disordered films was in the early 1979 on quench condensed Pd [158]. This was before the theoretical discovery of weak localization. The appearance of the theory of the magneto-resistance of QUIAD stimulated, of course, the experimental investigations. Besides the MOS inversion layers which are not discussed here, most of the experiments concentrated on Cu-films [90, 94, 105, 108–109, 121], Ag-films [103, 105, 112], Au-films [99, 105, 107, 112], Mg-films [92, 96–98, 116, 119, 127], Bi-films [104, 111, 114, 121], Pd and PdAu alloy-films [95, 122] and Pt-films [101, 132] and indium oxide films [89, 91, 124]. The experimental results show considerable differences. For example some of the Cu-films showed for all temperatures above 4 K a negative magneto-resistance [94, 90] while others [105, 108, 159] possess a positive magneto-resistance at low fields and low temperatures (4.2 K). Abraham and Rosenbaum [109] found both kinds of behaviour depending on the thickness of the Cu-film. Also the temperature dependence of the magneto-resistance is quite different for different authors. Van Haesendonck et al. [90] and Abraham and Rosenbaum [109] observed only a weak temperature dependence below 20 K. It is generally believed that the missing temperature dependence is caused by magnetic impurities. In fig. 5.1a–c some experimental results by

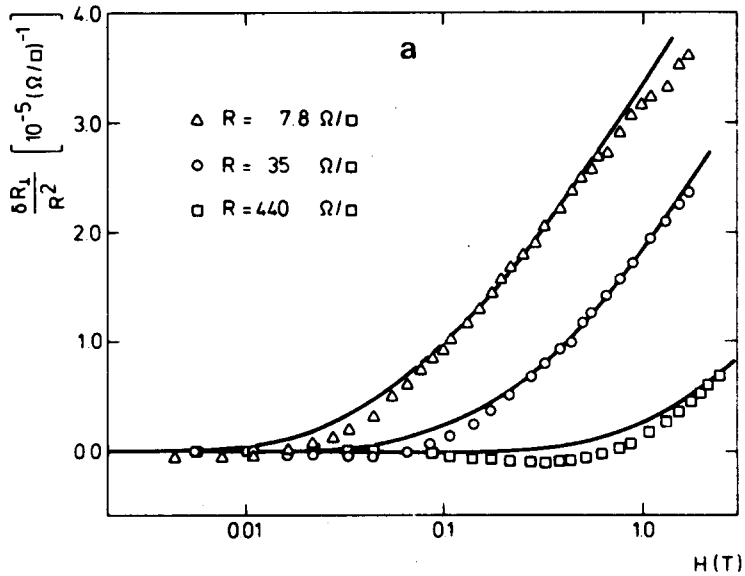


Fig. 5.1(a).

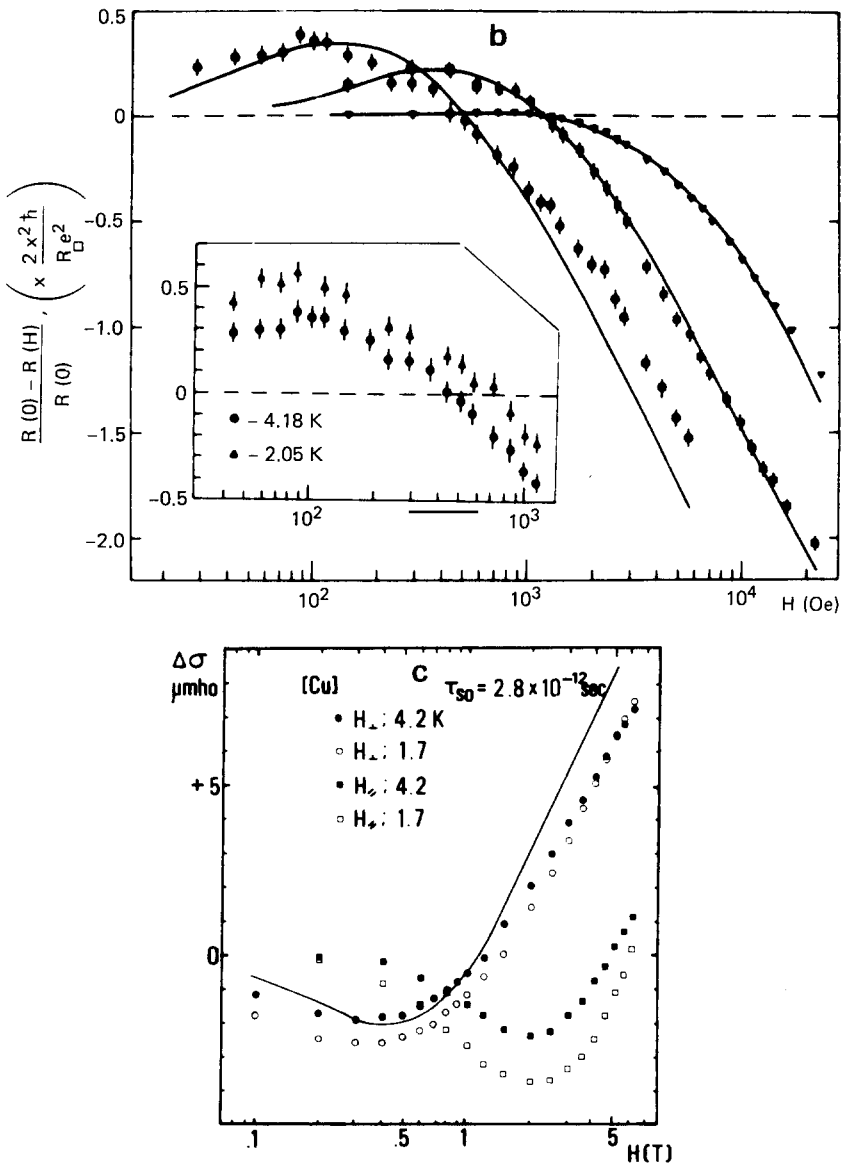


Fig. 5.1. The magneto-resistance (or magneto-conductance respectively) of a thin Cu-film, (a) from van Haesendonck et al. [90], (b) Gershenson and Gubankov [100], (c) Komori et al. [159]. The points are experimental results and the full curves theoretical ones.

van Haesendonck et al. [90], Gershenson and Gubankov [108] and Komori et al. [159] are shown. The full curves represent the theory.

For heavier metals like Ag, Au, Pd, Pt and Bi one observes in all investigated films at low temperatures and low fields a positive magneto-resistance demonstrating the dominant role of the spin–orbit scattering. Fig. 5.2 shows the results by Gershenson et al. [103] on Ag and fig. 5.3 reproduces the magneto-resistance on Au measured by Kawaguti and Fujimori [112]. For both measurements one recognizes a very good agreement between experiment and theory. A similar good agreement has been observed for Bi-films by Komori et al. [111] and Woerlee et al. [114]. As has been pointed out in section

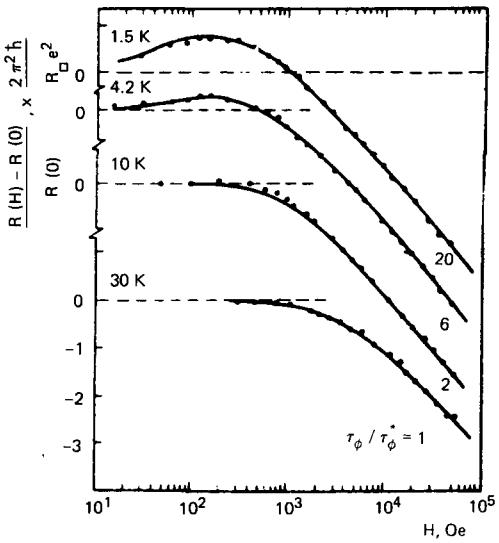


Fig. 5.2. The magneto-resistance of a thin Ag-film taken from Gershenson et al. [103]. The points are experimental results and the full curves theoretical ones.

2 the author found also very good agreement between experiment and theory for quench condensed Mg, Cu, Ag and Au. The only system where the author found clear deviations between experiment and theory until now is Pd. Pd shows a strong positive magneto-resistance but even with infinite large spin–orbit scattering it is not possible to reproduce the experimental points with theory. It is probable that the deviation is caused by the nearly ferromagnetic behaviour of Pd. The applied magnetic field may change the inelastic lifetime.

One important check of the theory of weak localization is the anisotropy of the magneto-resistance. The magneto-resistance for fields parallel to the film should be much smaller than perpendicular to the

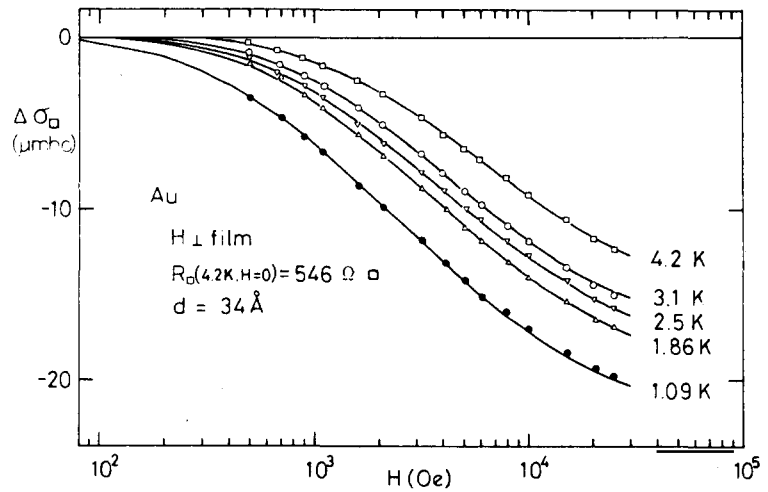


Fig. 5.3. The magneto-resistance of a thin Au-film taken from Kawaguti and Fujimori [173]. The points are experimental results and the full curves theoretical ones.

film [27]. This anisotropic behaviour has been observed in many thin films [90, 108–109, 112, 159, 101, 99, 122, 111, 104, 114, 91].

At this point it appears reasonable to discuss the evaluation of experimental curves in some detail. We have two different cases: (a) the magneto-resistance is for all fields positive or negative, (b) the magneto-resistance changes sign as function of the magnetic field. In the latter case it must be positive at small fields and negative at large fields. (In this discussion we assume that the magneto-resistance is only due to weak localization. Other magneto-resistance effects such as the classical one can complicate the evaluation or can even make it impossible.) In the second case one determines independently the spin–orbit scattering time and the phase coherence time (inelastic lifetime). Of particular importance is the quadratic field dependence at low fields and the position of the maximum. Generally it is not possible to analyse the phase coherence time in terms of the inelastic lifetime and the magnetic scattering time. Every metal contains more or less magnetic impurities which destroy the phase coherence of the two interfering (complementary) waves after roughly the time $\tau_s$ (see below). One can easily extract from the theoretical formula of the magneto-resistance [105] that it is hardly possible to separate the two mechanisms. Therefore in the evaluation of the experiment one determines an effective inelastic lifetime and has afterwards to discuss a possible magnetic origin. This is particularly difficult if the inelastic lifetime changes the power-law of its temperature dependence. On the other hand the effect of magnetic impurities can be erroneously interpreted as a change of the power-law of $1/\tau_i(T)$. The evaluation of the first case with a monotonous magneto-resistance is even more difficult. Here the measurement does not allow an independent determination of the inelastic lifetime and the spin–orbit scattering time [105]. If one has the possibility to change the spin–orbit scattering time during the experiment then one can evaluate the experimental data, otherwise an independent determination of $\tau_i$ and $\tau_{so}$ is not possible. Of course the difficulty of the distinction between $\tau_i$ and $\tau_s$ remains.

The main information on the experimental magneto-resistance comes from the low-field behaviour. There is no reliable determination of $\tau_i$ if the low-field part is not accurately measured. The high-field behaviour of the magneto-resistance is less well described by the theory. This has several reasons. First in a high magnetic field the coherence of the complementary waves is already destroyed after the relative short time $t_H = \hbar/(4eDH)$. For sufficient high fields the film is no longer two-dimensional when $d^2 \approx Dt_H$. Therefore a thin film does not show a $\ln(H)$-dependence of the magneto-resistance in high fields. One can, however, take care of this high-field deviation by summing over finite $k_z$-planes in $k$-space. The second high-field difficulty is more serious. In the derivation of the theory one restricted the calculation to a $q^2$-expansion, all higher powers of $q$ have been neglected. Therefore the derivation is only applicable for small $q^2$. Since $q^2$ corresponds to $(n+\frac{1}{2})4eH/\hbar$ the final formulae for the magneto-resistance apply only to fields which are not too large (the actual deviation at high fields is difficult to calculate).

Furthermore at high fields the electron–electron interaction which we will discuss in section 7 may cause a magneto-resistance. According to Lee and Ramakrishnan [33] one expects a positive magneto-resistance at fields of the order of $[2\mu_B/k_BT]^{-1}$. Generally this contribution is completely negligible in the interesting field range of QUIAD. In addition a strong spin–orbit scattering should destroy this magneto-resistance and a recent calculation by Finkelstein [160] suggest that a repeated electron–electron interaction has to be taken into account.

### *5.4. Magnetic impurities*

The QUIAD allows to study the properties of magnetic impurities because the magnetic scattering

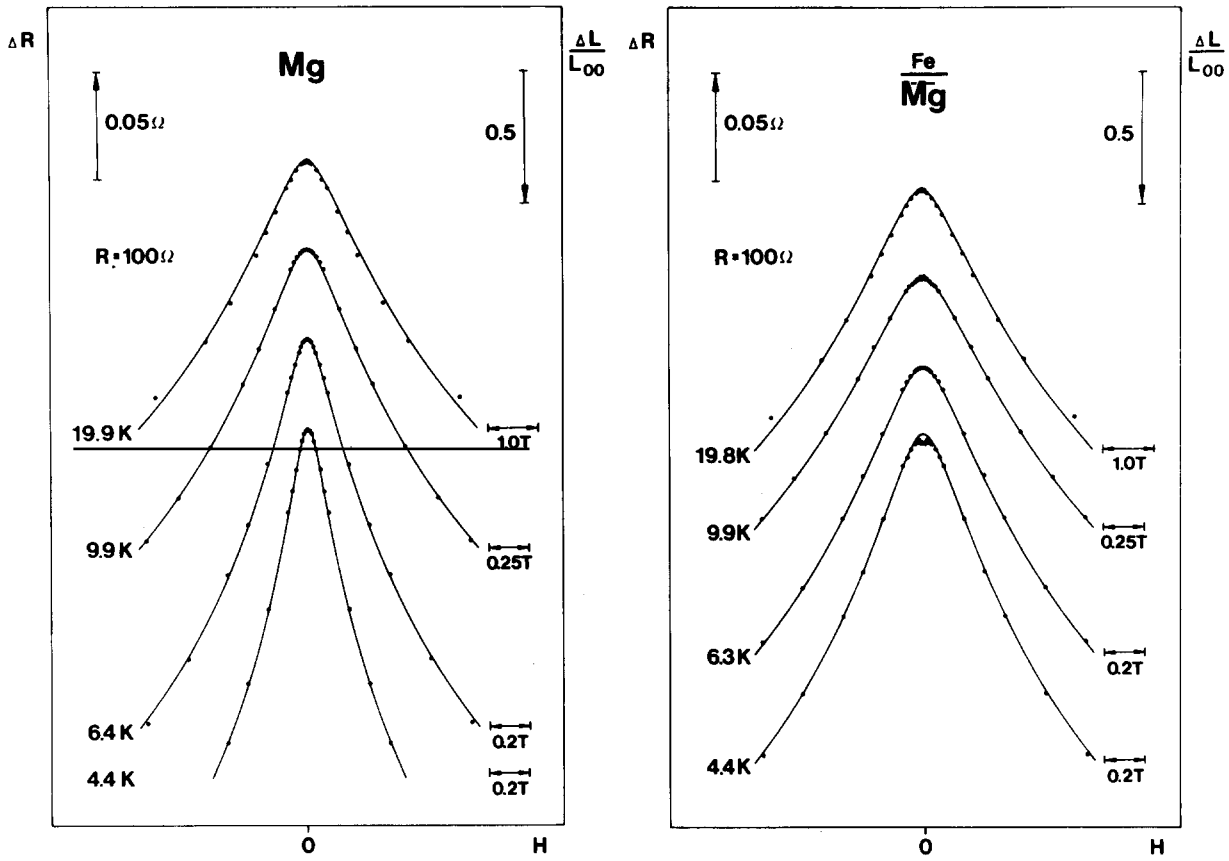


Fig. 5.4(a, b). The magneto-resistance curves of a thin Mg-film before and after the coverage with about 1/1000 layer of Fe. The points are experimental results and the full curves theoretical ones.

brings the two complementary waves out of phase and the magneto-resistance yields the magnetic scattering time as a function of temperature. This effect is frequently an undesired disturbance in the investigation of so-called "pure" films as discussed above.

The physical reason for the destructive influence of magnetic impurities is quite interesting. We consider the motion of the two complementary waves in real space (fig. 2.5). The partial wave which propagates along the first path is scattered by magnetic impurities along its way and exchanges spin with the localized magnetic impurities. During this propagation the spin of the electron is rotated during each "spin-flip process" by a small angle in space (the total spin function which is the sum of the potential scattering and the spin-flip scattering is only slightly tilted during such a process). The complementary electron wave which passes the impurities in opposite direction meets the magnetic impurities in the same original orientation. Only such processes which generate the same "spin-flips" at the magnetic impurities can contribute to the interference. For these processes the partial electron wave experiences the same spin rotation as the former complementary wave. However, this rotation occurs in the opposite sequence. Since the three-dimensional rotations do not commutate (this is a non-Abelian group) the two final spin states are not the same and the interference is progressively destroyed.

The author [98] studied the influence of Fe on the magneto-resistance of Mg. First a thin Mg-film has been investigated and its inelastic lifetime (and spin–orbit scattering time) has been determined.

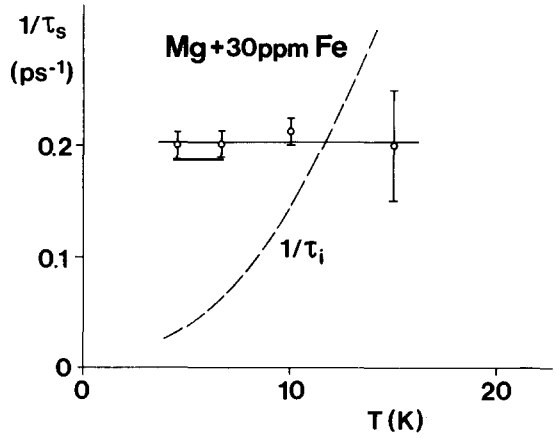


Fig. 5.5. The inverse magnetic scattering time of Mg with about 30 ppm Fe as a function of the temperature.

Afterwards the Mg-film has been covered with about 1/1000 layer of Fe. Since only the magnetic scattering time, i.e. the corresponding field $H_s$, is changed the evaluation allows an unambiguous determination of $H_s$ or $\tau_s$ respectively as a function of temperature. Fig. 5.4a shows the magneto-resistance curves of the Mg before and fig. 5.4b after the coverage with Fe. Again the full curves are obtained from the theory. In fig. 5.4b only $H_s$ had to be adjusted. Fig. 5.5 shows $1/\tau_s$ as a function of temperature for Fe in Mg. Here the Fe has been buried by another five layers of Mg.

In this case the Fe is a "bulk" impurity. Often one finds for bulk magnetic impurities an interesting deviation from the theory. The magneto-resistance shows a small minimum at zero field which has nothing to do with spin–orbit scattering. It might be caused by the interaction of the Fe-atoms or by a Kondo behaviour which takes multiple scattering of the conduction electron by one magnetic impurity into account [67]. This effect has also been seen in thin Cu-film with about 10 ppm Fe. The effect of magnetic impurities is only little explored and promises new basic insight into the physics of magnetic impurities. For example there is yet no direct experimental verification of the temperature dependent magnetic scattering time in Kondo systems. Weak localization provides a method for its measurement.

### *5.5. Spin–orbit scattering*

The importance of spin–orbit scattering on QUIAD has been discussed in section 2. We have seen that a superposition of Mg with Au allows a controlled change of the spin–orbit scattering. With such an experiment one can examine the consistency of the magneto-resistance [116]. In fig. 2.11 the magneto-resistance curves of a pure Mg-film were plotted for different temperatures. Fig. 5.6 shows the magneto-resistance of the same Mg-film with a coverage of 1/4 layer of Au. The two sets of curves in fig. 2.11 and fig. 5.6 are calculated for each temperature with the same value of $H_i(T)$ (or $\tau_i$ respectively) and each set is calculated with the same $H_{so}$. This means that the two sets of curves differ just by one parameter; the spin–orbit scattering which is modified by the additional Au. This demonstrates the high degree of consistency between experiment and theory.

Concerning the spin–orbit scattering time $\tau_{so}$ systematic work has still to be done to investigate the dependence on different metals as well as on the structure of the film, i.e. its defects. Here one has to keep in mind that only the non-periodic part of the spin–orbit coupling potential of the atoms contribute to the spin–orbit scattering (the periodic part is absorbed in the Bloch wave function of the electron).

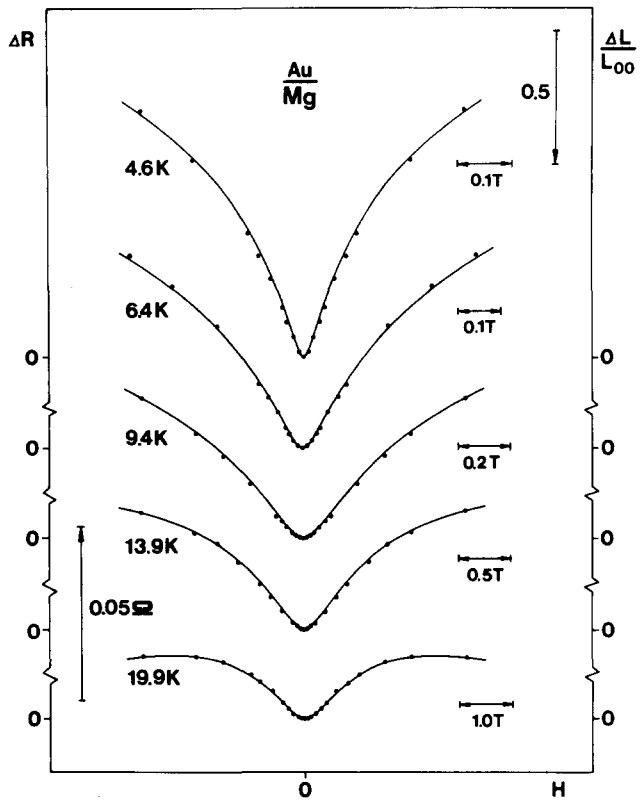


Fig. 5.6. The magneto-resistance of the same Mg-film as in fig. 2.11 after superposition with 0.25 atola of Au. The units of the magnetic field are the same as in fig. 2.11. The points represent the experimental results. The full curves are calculated with the same set of $H_i(T)$ as in fig. 2.11 and the new value $H_{so} = 0.54$ T.

## 5.6. *Temperature dependence of the resistance*

The first prediction of the theory of weak localization was the logarithmic anomaly of the resistance with temperature [2, 4]. As shown in fig. 2.4 such a resistance anomaly has been observed experimentally by several authors [85, 87, 86] shortly after the theory was worked out. However, at about the same time Altshuler et al. [12] showed that the dynamic modification of the electron–electron interaction in disordered metals yields in two dimensions a very similar anomaly of the resistance (see section 7).

First the two theoretical predictions have been considered as alternatives. However, after the first magneto-resistance measurements it became clear that both effects coexist. On the other hand the spin–orbit scattering should modify or even invert the contribution of weak localization. For example the measurements by Dolan and Osheroff [85] used Au/Pd alloys in which the spin–orbit scattering should dominate and the theory of weak localization predicts in this case a logarithmic decrease of the resistance with decreasing temperature. Therefore the original interpretation became doubtful and the investigation of the magneto-resistance was much easier to interpret.

On the other hand magneto-resistance measurements in small fields yield the inelastic lifetime $\tau_i(T) \approx T^{-p}$ and the spin–orbit scattering time $\tau_{so}$. Therefore one knows the relevant parameters of weak localization and their temperature dependence. This allows to calculate the temperature dependent contribution of weak localization to the resistance. If one considers a two-dimensional system in

which the spin–orbit scattering is changed from 0 to infinity while the temperature dependent inelastic lifetime is not altered then the temperature dependent correction of the conductance $\Delta L_{\omega 1}$ changes sign and reduces by a factor of 1/2. Experimentally this manipulation of the spin–orbit scattering can be achieved by superimposing Mg with a fraction of a monolayer of Au. In fig. 2.11 and fig. 5.6 the magneto-resistance curves of such a thin film have been shown. For the same system the author [116] measured also the temperature dependence of the pure Mg-film and the Mg covered with 1/4 layer of Au. The temperature dependence of the resistance is shown in fig. 5.7. Obviously one finds the strong influence of the spin–orbit scattering.

From the evaluation of the magneto-resistance measurements we know the temperature dependence of $H_i(T)$. Together with the two values of $H_{so}$ we can calculate the temperature dependence of the resistance which is caused by weak localization. This is, of course not the only contribution to the temperature dependence of the resistance. In addition we have the Altshuler contribution caused by the electron–electron interaction and (at higher temperature) the thermal part. But when we take the difference in the resistance between the Mg- and the MgAu-film then the other contributions should cancel and we can check whether the temperature dependence of weak localization also obeys the theory. Both, the experimental differences and the theoretical ones using $H_i(T)$ and the two $H_{so}$ values, are plotted in fig. 5.8. There is a good agreement between experiment and theory which demonstrates

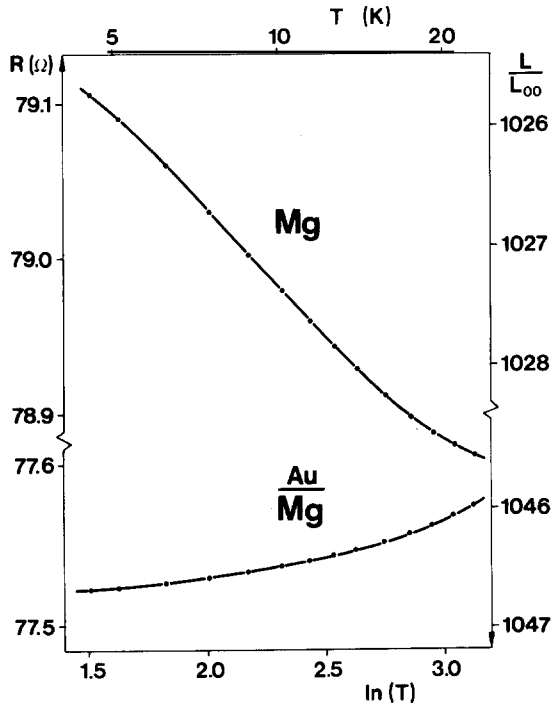


Fig. 5.7. The resistance (i.e. the normalized conductance $L/L_{\infty}$ using the right scale) as function of $\ln(T)$ for a Mg-film with a thickness of 84 Å. The same measurement after a superposition with 0.25 atola Au and another annealing at 40 K.

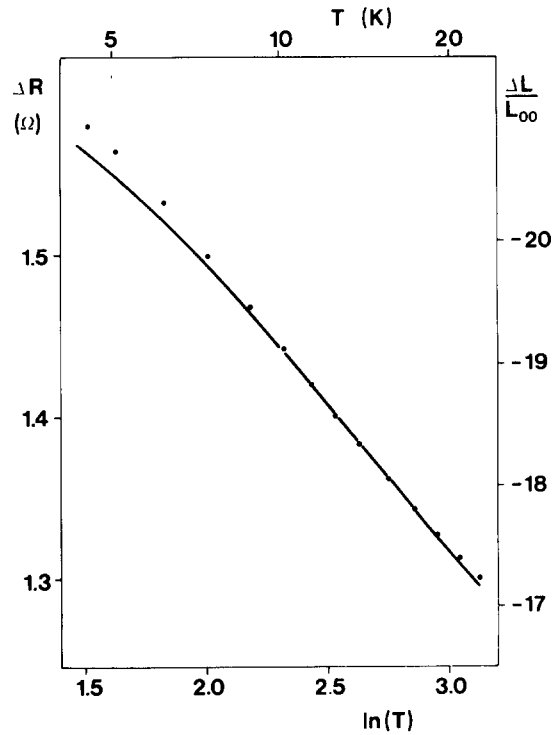


Fig. 5.8. The difference between the measured resistance of the Mg- and the MgAu-film as a function of temperature (circles). The full curve gives the theoretical differences between the corresponding conductance (right scale) of the Mg- and the MgAu-films using the common set of $H_i(T)$ and the two different values of $H_{so}$ which are evaluated from the magneto-resistance in fig. 2.11 and fig. 5.6.

that also the temperature dependence of the resistance is consistant with the theory of weak localization but it is much more complicated than the $\ln(T)$ anomaly predicted by the first theories.

### 5.7. *Influence of an electrical field*

While the effect of a magnetic field on weak localization is indisputable and experimentally proved the influence of an electric field on weak localization was quite controversial. It was discussed in the theoretical papers by Tsuzuki [39] and Altshuler and Aronov [6]. They obtained contrary results. Tsuzuki predicted a reduction of the quantum correction in an electric field. The result by Altshuler et al. is that – as long as the temperature is constant – the electric field has no influence on weak localization. These different theoretical results are not just due to different approximations or trivial errors but a consequence of the generalization of the equation of motion of the so-called Cooperon in the presence of a time-dependent vector potential. While Tsuzuki replaced the momentum $\boldsymbol{q}$ by $-i\nabla - (2e/\hbar)\,\boldsymbol{A}(\boldsymbol{r}, t)$, Altshuler et al. used an equation which is not instantaneous in time. In addition Kaveh et al. [161] assumed that the electric field $F$ introduces a characteristic length $X_F = (\hbar D/eF)^{1/3}$ which destroys weak localization as soon as $X_F$ becomes smaller than the Thouless length $(D\tau_i)^{1/2}$ in analogy to the characteristic length in a magnetic field $X_H = (\hbar/eH)^{1/2}$. This yielded roughly the same result as Tsuzuki's theory.

An experimental decision had therefore an important impact on the theory of weak localization. Experimentally an influence of the electric field on the conductance has been measured in thin films [85, 101]. The first measurement by Dolan and Osheroff [85] has been interpreted by Anderson et al. [2] as a heating of the conduction electrons by the current. This is the general difficulty in the experimental investigation that a large electric field causes also a considerable heating of the conduction electrons and one has to assure that the conduction electrons remain at constant temperature. Fortunately the magneto-resistance of weak localization allows us to control the electronic temperature. The magneto-

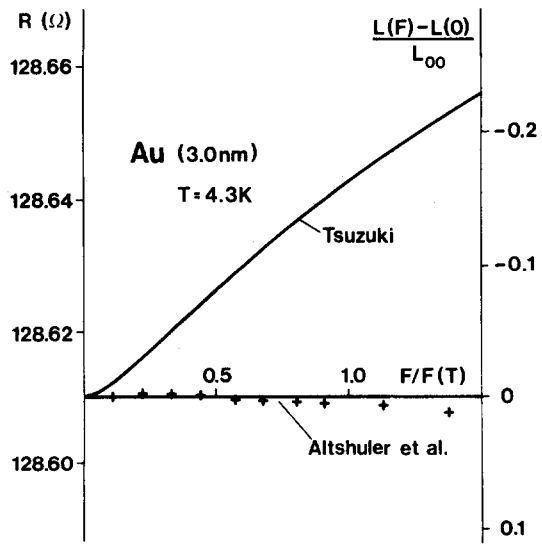


Fig. 5.9. The change of resistance or conductance respectively as a function of the electric field at constant temperature. Experimentally there is no change with electric field. The full curve gives the prediction of the theory of ref. [39].

resistance is determined by $H_{so}$ and the temperature dependent $H_i(T)$. If one measures the magneto-resistance with different electric currents (i.e. electric fields) and obtains identical magneto-resistance curves then the electronic temperature is not raised by the current. For this purpose one needs a very thin film which is embedded in liquid helium. This provides an optimal cooling of the film. Such a measurement [107] confirms the theory by Altshuler and Aronov. Fig. 5.9 shows the resistance of an Au-film 30 Å thick as a function of the normalized electric field $F/F(T)$. Here $F(T)$ is given by the relation:

$$F(T) = F_0 * (H_i/H_o)^{1.5}; \qquad F_0 = 6^{1/2}\hbar/(l\tau_0 e)$$

where $H_i$ is obtained from the magneto-resistance and $H_o$ from the resistivity of the film. (In the plot the experimental value for $F(T)$ was used: $F(4.3\,\mathrm{K}) = 271$ V/m.) On the right $y$-axis the corresponding unit for the electro-conductance $[L(F) - L(F=0)]/L_{00}$ is given. The resistance is with high accuracy independent of the electric field in a field range where refs. [39] and [161] predicted a field dependence.

## 6. The inelastic lifetime $\tau_i$

Anderson et al. [2] and Gorkov et al. [4] introduced the inelastic lifetime $\tau_i$ of the conduction electrons in weak localization. They calculated the frequency dependent conductance at $T = 0$ and replaced $\omega$ by $\omega + i/\tau_i$. Considering the physics behind weak localization one realizes that the quantum interference is destroyed when the two complementary scattering series (′) and (″) loose their phase-coherence. This may take place within the time $\tau_\varphi$, the phase-coherence time. The time $\tau_\varphi$ is in principle not identical with the inelastic lifetime $\tau_i$. Experimentally it became a custom to talk about the inelastic field or the inelastic lifetime respectively. So whenever an experimentally determined time is called inelastic lifetime the phase-coherence time $\tau_\varphi$ is meant.

### *6.1. Experimental results*

Although weak localization provides a unique method to determine the phase-coherence time of conduction electrons the experimental results are only fragmentary until now. The number of metals studied so far is very limited and mainly restricted to Mg, the noble metals, Bi and Pd. There is little systematic study of the dependence of $\tau_i$ on the film thickness and the mean free path of the conduction electrons. Even the temperature dependence is not always clear. The latter is due to the fact that other phase breaking mechanisms such as magnetic scattering can hardly be separated from the temperature dependent inelastic lifetime. Therefore in some experimental work an additional temperature independent phase breaking is assumed to recover a simple power law for $\tau_i$. Even non-magnetic impurities like co-evaporated air can dramatically enhance the phase breaking and remove its temperature dependence. Therefore it should be notified before the experimental results are reviewed that most of the work has still to be done.

The first and most interesting question is the temperature dependence of $1/\tau_i$ which is assumed to behave as $T^p$. Therefore the experimentally determined times are first examined in a log–log-plot versus temperature. The exponent does not depend on the exact value of $H_n\tau_n$ which requires the exact thickness of the film and the density of states.

Gershenzon et al. [103] found for Ag $p = 2.25$ (see fig. 6.1). In their films they found deviations from this law below 4 K and below 10 K respectively which are probably caused by magnetic scattering.

Kawaguti and Fujimori [112] observed for Ag and Au as well a power-law for $1/\tau_i$ with $p = 1$ in the temperature range between 1 and 4.2 K. This is shown in fig. 6.2. They saw a tendency for a stronger temperature dependence at higher temperatures.

Komori et al. [162] determined the inelastic lifetime for Bi-films and found a change of $p$ from 2 above 1 K to $p = 1$ below 1 K.

Woerlee et al. [114] observed qualitatively the same result for Bi-films, but did not explicitly give the range of $p$.

Abraham and Rosenbaum [109] measured for Cu above 30 K a $T^2$-law. Below 10 to 20 K the phase coherence time becomes temperature independent. Fig. 6.3 shows their effective field which is a sum of $H_i$ and $H_s$.

For quench condensed Mg the author [96, 116] found a $T^2$-law for $1/\tau_i$ in the temperature range between 4.5 and 20 K (see fig. 2.12). For the noble metals [105, 116] a power-law with $p \approx 1.7$ was seen but a larger value of $p$ which is hidden by a very weak temperature independent phase-breaking cannot be excluded.

Recently White et al. [127] extended similar measurements on Mg down to temperatures of 0.15 K. They used also quench condensed films but their mean free path is by more than a factor of ten smaller indicating a co-condensation of rest gas in the system. They interpret their low temperature results with a $T^1$-law but their data can easily be interpreted with $p = 1.5$ and additional magnetic scattering which flattens the curve at low temperature. Deutscher et al. [119] measured the inelastic lifetime of Mg evaporated at room temperature. They found for $p$ a transition from about 2 at temperature above 5 to 10 K to smaller $p$ at lower temperatures. However, for some of their films the temperature dependence of $1/\tau_i$ turns towards a constant so that an influence of magnetic scattering cannot be excluded.

Ovadyahu [124] saw for indium-oxide films a $T^1$-law for $1/\tau_i$.

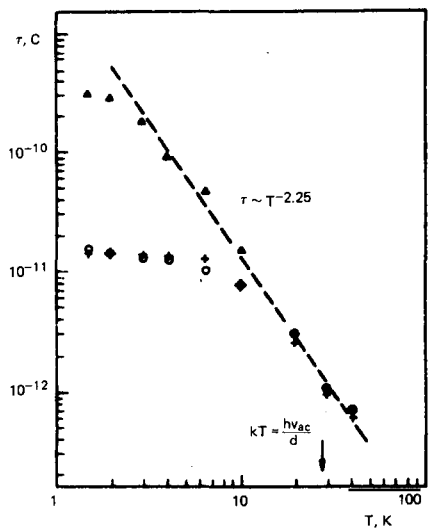


Fig. 6.1. The inelastic lifetime of an Ag-film, measured by Gershenson et al. [103] as a function of temperature.

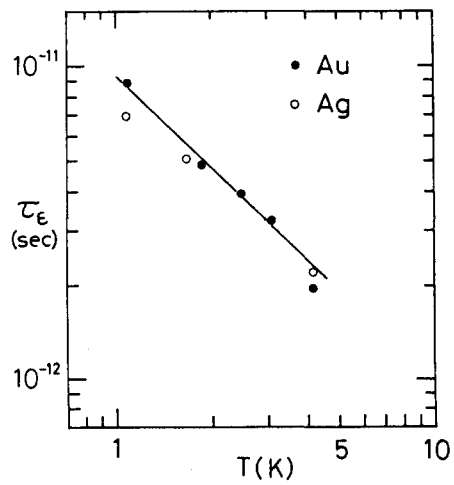


Fig. 6.2. The inelastic lifetime of an Ag- and Au-film, measured by Kawaguti and Fujimori [112] as a function of temperature.

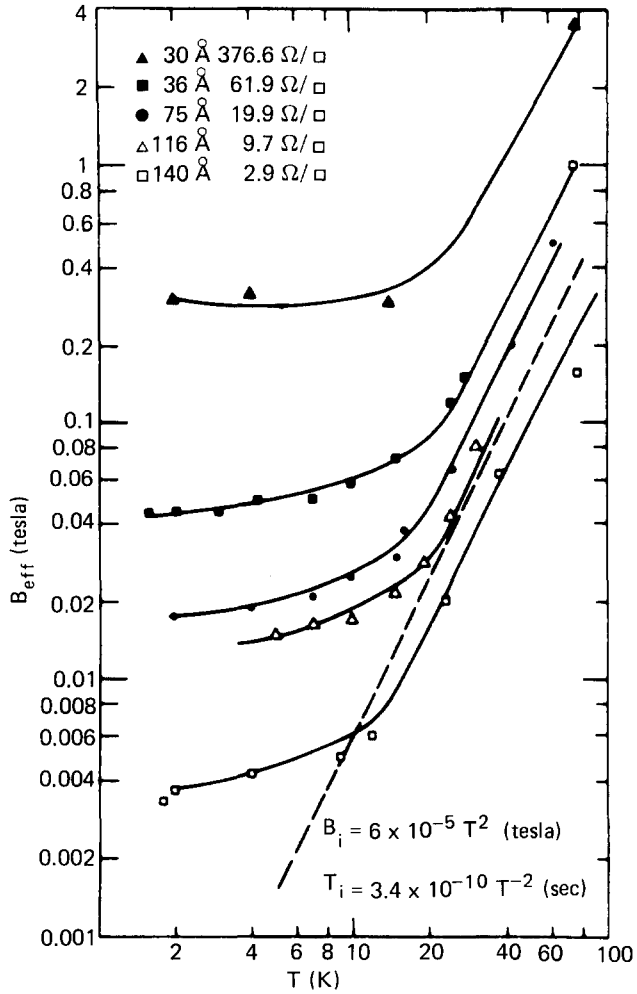


Fig. 6.3. The characteristic field of Cu-films (which is roughly a sum of $H_i$ and $H_s$), measured by Abraham and Rosenbaum [109] as a function of temperature.

## 6.2. *Theory of phase-coherence time*

The calculation of the phase coherence time is much more difficult than the calculation of the inelastic lifetime [45]. In this section we first list the theoretical results for the inelastic lifetime in pure and dirty metals and its temperature dependence – in particular the exponent $p$. We have to discuss electron–electron interaction and electron–phonon interaction.

(1) *Electron–electron interaction.*

According to Schmid [163] the inverse inelastic lifetime of an electron due to electron–electron interaction is modified in a (three-dimensional) metal with finite mean free path of the electrons. He obtained for an electron with an energy $E$ above the Fermi energy (at $T = 0$)

$$\frac{1}{\tau_i} = \frac{\pi}{8}\frac{E^2}{E_F} + \frac{3}{2}\left(\frac{1}{kl}\right)^{3/2}\frac{E^{3/2}}{E_F^{1/2}}. \tag{6.1}$$

The inelastic lifetime at finite temperature is essentially obtained by replacing $E$ by $k_B T$. A similar form has been derived by Altshuler et al. [6] (although it differs by a constant factor of the order of 10). The impurity induced contribution of the electron–electron interaction to $1/\tau_i$ generally varies in 3 dimensions as $T^{-1.5}$. Two-dimensional calculations have been performed by a number of authors [164, 26, 63, 165, 45, 66]. For a thin film Abrahams et al. [164] derived a $T * \ln(T)$ dependence for the impurity term of $1/\tau_i$. Fukuyama and Abrahams [66] repeated the calculation for the physically relevant phase coherence time $\tau_\varphi$ and obtained

$$1/\tau_\varphi = (\pi/k_F d)\,(k_B T/2E_F\tau_0) * \ln(T/T_1) \tag{6.2a}$$

where the $T_1$ is given by

$$k_B T_1 = (32/27)\,(k_F l)^3\, E_B$$

where $E_B$ is the Bohr energy (13.6 eV or $1.57 \times 10^5$ K respectively). Altshuler et al. [26, 45] did not find the $\ln(T)$-term in the $\tau_\varphi$, which they calculated as the Nyquist time $\tau_N$,

$$\hbar/\tau_N = (k_B T/2\pi DNd) * \ln(k_B T\tau_N/\hbar) \tag{6.2b}$$

which differs from eq. (6.2a) because it has no $\ln(T)$-dependence. Lopes dos Santos [77] recovered essentially the result by Abrahams et al. modified by a factor of two.

(2) *Electron–phonon interaction.*

The electron–phonon interaction is also enhanced by impurities, i.e. a finite mean free path of the conduction electrons. This has been first derived by the author [81, 166–167] who modified the Anderson theorem that impurities do not change the transition temperature of a superconductor, pointing out that the impurities participate in the lattice oscillations (i.e. the phonons) and change the electron–phonon interaction. Within this picture the Eliashberg function $\alpha^2 F(E)$ in a disordered metal was calculated [167] to explain the enhanced superconductivity and the strong coupling behaviour of quench condensed superconductors. Schmid [168] derived in a jellium model the inelastic lifetime of the conduction electron at $T = 0$. Takayama [169] calculated the temperature dependence of the resistance.

The author obtained for the impurity correction of the Eliashberg function

$$\alpha^2 F(E) = \frac{\hbar n}{4\pi LMm}\,|c^{-3}|_{av}\,\frac{E}{l} \tag{6.3}$$

where $n$ is the electron density, $L$ the number of atoms per volume, $M$ the ion mass, $m$ the electron mass and $(1/c^3)_{av}$ an average over the sound velocities. This yields for the temperature dependence of the inelastic lifetime according to the relation [170]

$$\begin{aligned} \frac{1}{\tau_i} &= \frac{4\pi}{\hbar}\int \frac{dE\,\alpha^2 F(E)}{\sinh(E/k_B T)} \\ \frac{1}{\tau_i} &= \frac{n}{LMm}\left(\frac{1}{c^3}\right)\frac{1}{l}(k_B T)^2 \int_0^\infty \frac{x\,dx}{\sinh(x)}. \end{aligned} \tag{6.4}$$

The integral yields the numerical value 2.47. Schmid [168] found first no linear energy dependence of the Eliashberg function and derived an $E^3$ and an $E^4$ term in the inelastic lifetime. As a consequence the temperature dependence of $\tau_i$ should show the same exponents $p = 3$ and 4. Later Keck and Schmid [170] improved their calculation and for $\omega l/c > 1$ they obtained a term similar to that found by the author in the Eliashberg function. Takayama [169] also obtained an additional $T^2$ term for the inelastic lifetime in the presence of impurities.

The influence of the phonons on the electron phase raises still several questions. As we are going to discuss in section 7 the electronic screening in a disordered metal is retarded. One might expect that this causes a damping of the phonons which corresponds to an additional electron–phonon interaction. Another effect is that a phonon wave is accompanied by an oscillating electric field. The latter reduces according to Altshuler and Aronov [26] the phase coherence time of the conduction electrons.

### *6.3. Comparison between experiment and theory*

The experimentally determined exponents $p$ of the power-law are not really consistent with each other. There is, however, the general tendency that at temperatures above helium the exponent is of the order of two. The normal electron–electron interaction is by several orders of magnitude too small to explain the experimentally determined values of the inelastic lifetime. Only the impurity induced electron–electron interaction could be responsible. The exponent $p \approx 2$ is not in favour of the electron–electron interaction as the dominant inelastic scattering process. Even if the film is three-dimensional with respect to the electron–electron interaction one expects only an exponent $p = 1.5$. As a matter of fact some films are in the regime between two- and three-dimensional behaviour with respect to the electron–electron interaction. On the other hand the electron–phonon interaction neither gives a satisfying explanation for the $T^2$-law. For most of the films the product $q_T l$ is not larger than 1 in the temperature range of interest and only for $q_T l \gg 1$ the electron–phonon interaction experiences the different impurities independently.

Qualitatively it turns out that (above 4 K) the electron–phonon relaxation time is of the same order as the inelastic lifetime. The author [115] heated the conduction electrons in a thin Au-film by an electric current above the phonon temperature and investigated the electron temperature by means of weak localization. It turned out that the electron–phonon interaction is an important mechanism in determining the inelastic lifetime.

At low temperatures (below 2–4 K) there is some evidence (or at least no contradiction) that the dominant inelastic scattering mechanism is the electron–electron interaction. In this temperature range an exponent of the order of one has been observed [112, 127, 119] and White et al. [127] as well as Deutscher et al. [119] found a qualitative agreement with the theory of Abrahams et al.

At temperatures above 4 K both presently discussed mechanisms, the electron–electron interaction and electron–phonon interaction, fail to explain the experimental results. For both, the inverse inelastic lifetime should increase linearly with the disorder, i.e. proportional to the resistivity. This is experimentally not the case [105].

We compare the magnitude of the measured inelastic lifetime with the different theoretical models. The author [105] has performed such a discussion for the inelastic lifetime of Cu at 10 K. The experimental value for $\tau_i$ at this temperature is about $5 \times 10^{-12}$ s [105]. For the same temperature the theoretical models are evaluated. The inelastic lifetime due to the normal electron–electron interaction (yielding a $T^2$-law which is impurity and dimension independent) is of the order of $10^{-8}$ s. This contribution is too small. Secondly the impurity induced contribution of the electron–electron inter-

action to $1/\tau_i$ is estimated. If the film is considered as two-dimensional with respect to the electron–electron interaction the formula (6.2a) by Abrahams et al. can be applied. One obtains for $1/\tau_\varphi \approx 3 \times 10^{-11}$ s. The electron–phonon interaction according to eq. (6.4) yields for $\tau_i$ the value $4 \times 10^{-11}$ s. The value of $1/\tau_i$ is too small by a factor of about ten (and since $q_T l$ is not much larger than 1 the result is even over estimated). The discussed electron–electron interaction as well as the electron–phonon interaction are too small to explain the experimental result. But it is quite possible that the theory has not yet explored all possible mechanisms in the electron–phonon interaction.

We conclude this section with a number of questions which require further investigation.

(i) What is the power-law for $1/\tau_i$ in different regimes of temperature? (ii) How does $1/\tau_i$ depend on the resistivity and the film thickness? (iii) What is the role of surface scattering when the thickness is smaller than the mean free path? (iv) What is the actual mechanism in electron–phonon interaction that determines the inelastic lifetime?

## 7. Coulomb interaction

Resistance anomalies of thin films have been observed quite a few times in the past. For example Buckel and Hilsch [171] found already 25 years ago an increasing resistance with decreasing temperature in disordered Bi-films. Most of these anomalies can now be explained by the Coulomb anomaly of the resistance. As we mentioned below Altshuler et al. [157] predicted almost in coincidence with the theory of weak localization another very similar resistance anomaly as a function of temperature. The mechanism which causes the Coulomb anomaly is considerably more difficult than weak localization. The origin of this anomaly is the fact that the electron–electron interaction in disordered metals is retarded. A sudden change of the charge distribution in a disordered metal cannot be screened immediately. Since the electrons can only propagate by diffusion they need time to screen the charge distribution. Since the diffusion is particularly slow over large distances one finds a small screening for small $q$, i.e. a large effective electron–electron interaction. The result by Altshuler et al. for the effective Coulomb interaction in disordered electron systems is (for small $q$)

$$V_{sc} = \frac{1}{N} \frac{Dq^2 - i\omega}{Dq^2} \tag{7.1}$$

($N$ = density of states). The screening of a static potential is, however, hardly changed by impurities.

As a consequence of the exchange interaction every two electrons for example $\boldsymbol{k}'$ and $\boldsymbol{k}''$ perform transitions into the states $\boldsymbol{k}' + \boldsymbol{q}$ and $\boldsymbol{k}'' - \boldsymbol{q}$ and build up a finite amplitude for the final two-electron state. $q$ takes all possible values. This means that every two-particle state $|\boldsymbol{k}', \boldsymbol{k}''\rangle$ has a (two-particle) satellite state $|\boldsymbol{k}' + \boldsymbol{q}, \boldsymbol{k}'' - \boldsymbol{q}\rangle$ which is phase coherent. The two-particle states and their satellites are scattered by the impurities. There is a finite probability that the $|\boldsymbol{k}', \boldsymbol{k}''\rangle$ and $|\boldsymbol{k}' + \boldsymbol{q}, \boldsymbol{k}'' - \boldsymbol{q}\rangle$ are scattered into the same final two-particle state which we denote by $|\boldsymbol{k}, \boldsymbol{k} + \boldsymbol{q}\rangle$. (This scattering from $|\boldsymbol{k}'\rangle$ to $|\boldsymbol{k}\rangle$ and $|\boldsymbol{k}' + \boldsymbol{q}\rangle$ to $|\boldsymbol{k} + \boldsymbol{q}\rangle$ goes over a series of intermediate states with the same transfer of momentum.) In the final two-particle state the amplitudes have essentially opposite sign (because of the exchange); the amplitudes have preserved their coherence over a time of the order of $t_T = \hbar/(2\pi k_B T)$. Their "quantum interference" causes a correction to the resistance. The process is considerably more difficult than in weak localization and its physical interpretation shall be discussed elsewhere in detail.

The physics of the electron–electron interaction in disordered electron systems is a large field. I refer

the reader to two review articles on this field by Fukuyama [76] and Altshuler and Aronov [154]. In the present article we do not want to treat this field in any detail. However, an experimentalist is confronted with the fact that his measured temperature dependence of the resistance is not only determined by QUIAD but also by Coulomb interaction. Therefore this section is restricted to the resistance anomaly and the Hall anomaly which is closely related to the former and not influenced by weak localization. Many of the interesting consequences of the electron–electron interaction on density of states, thermo-power, tunneling resistance, etc. are not touched in this article.

### *7.1. Resistance anomaly*

Altshuler et al. [157] and Fukuyama [31] evaluated a Kubo graph which contained the dynamic Coulomb interaction and consisted of the Fock and of the Hartree term. They obtained a correction for the conductance

$$\Delta L(T) = -\Delta R/R_0^2 = -L_{00}(1-F)\ln(T)\,. \tag{7.2}$$

Here $F$ was originally defined as a screening factor,

$$F = [K/(2k_F)]^2 * \ln[1 + (2k_F/K)^2] \tag{7.2a}$$

where $K^{-1}$ is the screening length in three dimensions: $K^2 = Ne^2/\epsilon_0$ ($N$ = density of states at the Fermi surface). However, Finkelstein [160] showed recently that the Hartree term does not treat the Coulomb interaction consistently and $F$ had to be redefined. We will treat it as an adjustable parameter as it is in the experiment. The temperature dependence of the resistance is hardly influenced by a magnetic field. According to Fukuyama [44] the spin–orbit scattering modifies the anomaly slightly due to the Hartree contribution but again Finkelstein's results require a recalculation.

According to Lee and Ramakrishnan [33] the Hartree part of the Coulomb anomaly shows a (small) magneto-resistance. They obtained for the change of the conductance in a magnetic field

$$[L(H) - L(0)]/L_{00} = \begin{cases} (F/2)\,0.084\,h^2 & \text{for } h \ll 1 \\ (F/2)\ln[h/1.3] & \text{for } h \gg 1 \end{cases} \tag{7.3}$$

where $h = g\mu_B H/(k_B T)$.

The relation is only derived for vanishing spin–orbit scattering. For strong spin–orbit scattering ($1/\tau_{so} > 1/\tau_T$) the magneto-resistance vanishes. According to Finkelstein [160] one might expect that (7.3) must be modified.

There are also Kubo graphs which contain a combination of weak localization and electron–electron interaction. According to Altshuler et al. [21] one has to include the Coulomb interaction repeatedly. In a normal conducting metal the contribution of these "particle–particle diagrams" can be neglected.

Experimentally the Coulomb anomaly and the QUIAD anomaly are superimposed. One may separate the two contributions by applying a large magnetic field. The field suppresses the temperature dependence of the weak localization and only the Coulomb anomaly remains [104, 116]. Fig. 7.1 shows the experimental result by Komnik et al. [104]. The temperature dependent resistance is plotted for a Bi-film in different magnetic fields perpendicular to the film. Since Bi is a strong spin–orbit scatterer the contribution of weak localization and electron–electron interaction are opposite. The author [116]

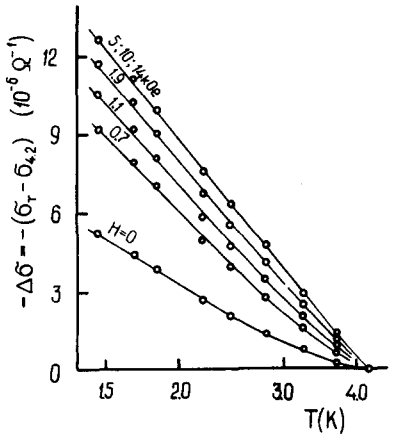


Fig. 7.1. The Coulomb anomaly of the resistance in a thin Bi-film according to Komnik et al. [104]. The resistance (negative conductance) is plotted for various magnetic fields perpendicular to the film. For large fields the temperature dependence of QUIAD is suppressed.

showed that the Coulomb anomaly is hardly changed by a change of the spin–orbit scattering. While Mg and Mg/Au have very different temperature dependences of the resistance in zero field (see fig. 5.8) the influence of the Au in a field of 7 T is negligible. The adjustable parameter $F$ is of the order of 0.2.

## 7.2. *Hall effect*

While the theory of weak localization predicts no change of the Hall constant [12, 11], Altshuler et al.

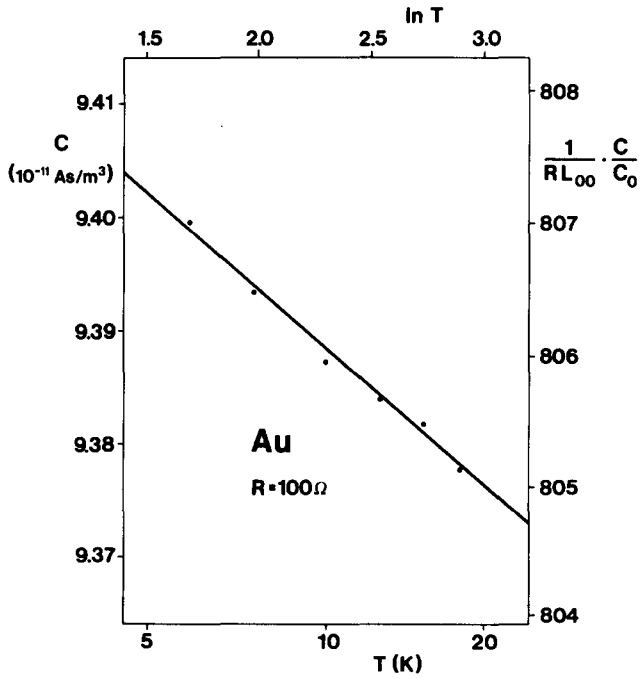


Fig. 7.2. The temperature dependence of the Hall constant for a thin Au-film [172].

[12] showed that the Coulomb interaction causes a clear change of the Hall constant with decreasing temperature. They obtained

$$\Delta C_C(T)/C_0 = 2\,\Delta R_C(T)/R_0 \tag{7.4}$$

(the index C stands for the correction caused by the Coulomb interaction). As a consequence of eqs. (7.2) and (7.4) one comes to the following:

$$\frac{\Delta C(T)}{C_0 R_0 L_{00}} = 2\,(1-F)\ln(T)\,. \tag{7.5}$$

The experimental difficulty for thin metallic films is that for reasonable film resistances the anomalies have a relative magnitude of $10^{-2}$ to $10^{-3}$. The Hall effect requires a measurement of a Hall angle of about $10^{-3}$ with an accuracy of about $10^{-4}$ which is rather tedious. Measurements of the temperature dependent Hall constant have been performed on electron inversion layers. There are only a few measurements on thin films; on the system $In_2O_3$, the semi-metal Bi and on thin Au-films. Ovadyahu and Imry [89] did not observe a temperature dependence of the Hall constant in thin $In_2O_3$-films. Woerlee et al. [114] measured the Hall constant at two different temperatures, at 4.2 K and 1.2 K. $C(T)/C_0$ increased by 1–2%. For thin Au-films the author [172] found an increase of the Hall constant with decreasing temperature as shown in fig. 7.2. The value of the adjusted parameter $F$ from the Hall effect measurement was 0.25.

## 8. Conclusions

In this article I tried to sketch the physical background of weak localization, its theoretical description and the experimental results presently existing. I wanted to point out that the phenomenon of QUIAD is well established and that careful experiments can be quantitatively reproduced by the theory if one fits the characteristic times of the electron system. This means that weak localization can be considered as a trustable and reliable experimental method to determine the characteristic times. It is a new experimental tool to study solid state physics in metals. And indeed there is a large number of problems waiting.

(1) The inelastic lifetime for different metals, its dependence on film thickness, mean free path, impurities, surface properties, etc.

(2) The magnetic scattering time for various magnetic impurities, Kondo impurities, mixed valences, van Vleck impurities, spin-glasses, etc. can be studied. The magnetic anomalies wait for their investigation.

(3) The measurement of the spin–orbit scattering opens another field of investigation. An old question is for example the Hall constant of liquid metals. Most simple liquid metals have a Hall constant which is simply given by the free electron value. However, the heavy metals like Pb, Bi, Tl show considerable deviations from the free electron value – in the liquid as well as in the amorphous state. It has been suggested that this deviation is due to spin–orbit scattering. However, the theoretical estimated value for $1/\tau_{so}$ appeared to be small and there was no way experimentally to measure it. Weak localization opens such a way for amorphous metals.

(4) Since the advanced evaporation technique allows to condense controlled impurities onto the surface and to cover them afterwards one can study whether the surface changes the properties of an

atom. The author observed for example that dilute Ni-atoms on the surface of Pd introduce a magnetic scattering which broadens the magneto-resistance curves. If one covers the Ni-atoms with a few layers of Pd then the magneto-resistance curves become as narrow as those for the pure Pd-film. The magnetic influence of the Ni-atoms has disappeared.

(5) The weak localization in sandwiches is theoretically not yet investigated. When such a theory exists one can experimentally investigate a large number of metals the investigation of which is difficult in a single film. Examples are superconductors or metal films with a very short inelastic lifetime. The latter can be "diluted" in a sandwich.

(6) In a superconductor one has besides weak localization and Coulomb anomaly a few other corrections to the conductance such as Aslamazov–Larkin and Maki–Thompson fluctuation and the Coulomb interaction in the two-particle channel. A quantitative analysis has only started [93, 106, 110, 113, 118, 125–126].

Therefore the investigation of the transport properties of thin films promises many further interesting results.

## Acknowledgement

The author would like to thank Prof. D. Rainer for many stimulating discussions and assistance in the theory.

## References

[1] E. Abrahams, P.W. Anderson, D.C. Licciardello and T.V. Ramakrishnan, Phys. Rev. Lett. 42 (1979) 673.
[2] P.W. Anderson, E. Abrahams and T.V. Ramakrishnan, Phys. Rev. Lett. 43 (1979) 718.
[3] F.J. Wegner, Z. Physik 35 (1979) 207.
[4] L.P. Gorkov, A.I. Larkin and D.E. Khmelnitzkii, Pis'ma Zh. Eksp. Teor. Fiz. 30 (1979) 248; JETP Lett. 30 (1979) 228.
[5] R.V. Haydock, Phil. Mag. B43 (1981) 203.
[6] B.L. Altshuler and A.G. Aronov, JETP Lett. 30 (1979) 482.
[7] S. Hikami, A.I. Larkin and Y. Nagaoka, Prog. Theor. Phys. 63 (1980) 707.
[8] R. Oppermann and K. Jüngling, Phys. Lett. 76A (1980) 449.
[9] K. Jüngling and R. Oppermann, Z. Physik B38 (1980) 93.
[10] A.I. Larkin, Pis'ma Zh. Eksp. Teor. Fiz. 31 (1980) 239; JETP Lett. 31 (1980) 219.
[11] H. Fukuyama, J. Phys. Soc. Jpn. 49 (1980) 644.
[12] B.L. Altshuler, D. Khmelnitzkii, A.I. Larkin and P.A. Lee, Phys. Rev. B22 (1980) 5142.
[13] D. Vollhardt and P. Wölfle, Phys. Rev. Lett. 45 (1980) 842.
[14] H. Aoki, J. Phys. C13 (1980) 3369.
[15] P.F. Maldague, Phys. Rev. B23 (1981) 1719.
[16] D.J. Thouless, Phys. Rev. Lett. 39 (1977) 1167.
[17] M.Y. Azbel, Phys. Rev. Lett. 46 (1981) 675.
[18] B.L. Altshuler and A.G. Aronov, Solid State Commun. 38 (1981) 11.
[19] B.L. Altshuler, A.G. Aronov and B.Z. Zpivak, JETP Lett. 33 (1981) 94; Pis'ma Zh. Eksp. Teor. Fiz. 33 (1981) 101.
[20] C.M. Soukoulis and E.N. Economou, Phys. Rev. Lett. 45 (1980) 1590.
[21] B.L. Altshuler, A.G. Aronov, A.I. Larkin and D. Khmelnitzkii, Sov. Phys. JETP 54 (1981) 411; Zh. Eksp. Teor. Fiz. 81 (1981) 768.
[22] M. Kaveh and N.F. Mott, J. Phys. C: Solid State Phys. 14 (1981) L183.
[23] P.A. Lee, J. Non. Crys. Sol. 35 (1980) 21.
[24] S. Maekawa and H. Fukuyama, J. Phys. Soc. Jpn. 50 (1981) 2516.
[25] K. Hillebrand and R.M. Nieminen, J. Phys. C14 (1981) L133.
[26] B.L. Altshuler and A.G. Aronov, Solid State Commun. 39 (1981) 619.
[27] B.L. Altshuler, A.G. Aronov and B.Z. Zpivak, JETP Lett. 33 (1981) 499; Pis'ma Zh. Eksp. Teor. Fiz. 33 (1981) 515.

[28] P.A. Lee and D.S. Fisher, Phys. Rev. Lett. 47 (1981) 882.
[29] Y. Ono, D. Yoashioka and H. Fukuyama, J. Phys. Soc. Jpn. 50 (1981) 2143.
[30] C.H. Hodges, J. Phys. C14 (1981) L247.
[31] H. Fukuyama, J. Phys. Soc. Jpn. 50 (1981) 3407.
[32] H. Fukuyama, J. Phys. Soc. Jpn. 50 (1981) 3562.
[33] P.A. Lee and T.V. Ramakrishnan, Phys. Rev. B26 (1982) 4009.
[34] S. Maekawa and H. Fukuyama, J. Phys. Soc. Jpn. 51 (1981) 1380.
[35] A. Kawabata, Solid State Commun. 38 (1981) 823.
[36] A. MacKinnon and B. Kramer, Phys. Rev. Lett. 47 (1981) 1546.
[37] H. Fukuyama, Surface Science 113 (1982) 489.
[38] J.L. Pichard and G. Sarma, J. Phys. C14 (1981) L617.
[39] T. Tsuzuki, Physica 107B (1981) 679.
[40] P. Wölfle and D. Vollhardt, Proc. 4th Taniguchi Int. Symp., Sanda-shi, Japan (1981) p. 26.
[41] C.S. Ting, A. Houghton and J.R. Senna, Phys. Rev. B25 (1982) 1439.
[42] H. Tagaki and Y. Kuroda, Sol. State Comm. 41 (1982) 643.
[43] D. Vollhardt and P. Wölfle, Phys. Rev. Lett. 48 (1982) 699.
[44] H. Fukuyama, J. Phys. Soc. Jpn. 50 (1982) 1105.
[45] B.L. Altshuler, A.G. Aronov and D.E. Khmelnitskii, J. Phys. C: Solid State Phys. 15 (1982) 7367.
[46] G. Bergmann, Solid State Comm. 42 (1982) 815.
[47] S. Hikami, Proc. 4th Taniguchi Int. Symp., Sanda-shi, Japan (1981) p. 15.
[48] T. Ando, Surf. Sci. 113 (1982) 182.
[49] A.A. Golub and V.P. Iordatii, Sov. Phys. Sol. State 24 (1982) 65.
[50] H. Kunz and B. Souillard, J. Phys. Lett. 43 (1982) L39.
[51] J.B. Pendry, J. Phys. C: Solid State Phys. 15 (1982) 4821.
[52] B.Z. Spivak and D.E. Khmelnitskii, JETP Lett. 35 (1982) 412; Pis'ma Zh. Eksp. Teor. Fiz. 35 (1982) 334.
[53] K.F. Berggren, J. Phys. C: Solid State Phys. 15 (1982) L843.
[54] J.B. Sokoloff and J.V. Jose, Phys. Rev. Lett. 49 (1982) 334.
[55] R. Oppermann, Solid State Commun. 44 (1982) 1297.
[56] Y. Ono, J. Phys. Soc. Jpn. 51 (1982) 2055.
[57] C.S. Ting, Phys. Rev. B26 (1982) 678.
[58] D.J. Thouless, Physica B and C 109 (1982) 1523.
[59] H. Fukuyama, J. Phys. Soc. Jpn. 52 (1983) 18.
[60] Y.C. Lee, C.S. Chu and E. Castano, Phys. Rev. 27B (1983) 6136.
[61] S. Maekawa, H. Ebisawa and H. Fukuyama, J. Phys. Soc. Jpn. 52 (1983) 1352.
[62] M. Ya. Azbel, Phys. Rev. B26 (1982) 4735.
[63] H. Ebisawa, S. Maekawa and H. Fukuyama, Solid State Commun. 45 (1983) 75.
[64] H. Fukuyama, Y. Isawa and H. Yasuhara, J. Phys. Soc. Jpn. 52 (1983) 16.
[65] B.L. Altshuler and A.G. Aronov, JETP Lett. 37 (1983) 175.
[66] H. Fukuyama and E. Abrahams, Phys. Rev. B27 (1983) 5976.
[67] F.J. Ohkawa, H. Fukuyama and K. Yosida, J. Phys. Soc. Jpn. 52 (1983) 1701.
[68] C.M. Soukoulis, J.V. Jose, E.N. Economou and P. Sheng, Phys. Rev. Lett. 50 (1983) 764.
[69] V.L. Bonch-Bruevich and A.L. Mironov, Phys. Stat. Sol. B114 (1982) 715.
[70] T.A.L. Ziman, Phys. Rev. B26 (1982) 7066.
[71] B.L. Altshuler and A.G. Aronov, Solid State Commun. 46 (1983) 429.
[72] H. Fukuyama, Proc. 4th Taniguchi Int. Symp., Sanda-shi, Japan (1981) p. 89.
[73] H. Tagaki, R. Souda and Y. Kuroda, Prog. Theor. Phys. 68 (1982) 426.
[74] D. Yoshioka, J. Phys. Soc. Jpn. 51 (1982) 716.
[75] U. Krey, W. Maass and J. Stein, Z. Physik B49 (1982) 199.
[76] H. Fukuyama, to be publ. in Modern Problems in Condensed Sciences.
[77] J.M.B. Lopes dos Santos, Phys. Rev. B28 (1983) 1189.
[78] W. Apel and T.M. Rice, J. Phys. C16 (1983) L271.
[79] M. Chaturvedi and V. Srivastava, Int. J. Quantum Chem. 23 (1983) 1463.
[80] A.A. Gogolin and G.T. Zimanyi, Sol. State Comm. 46 (1983) 469.
[81] D. Belitz, A. Gold and W. Götze, Z. Physik B44 (1981) 273.
[82] H. Ebisawa and H. Fukuyama, J. Phys. Soc. Jpn. 52 (1983) 3304.
[83] R. Oppermann, J. Phys. Soc. Jpn. 52 (1983) 3554.
[84] F.T. Vasko, JETP Lett. 35 (1982) 390; Pis'ma Zh. Eksp. Teor. Fiz. 35 (1982) 318.
[85] G.J. Dolan and D.D. Osheroff, Phys. Rev. Lett. 43 (1979) 721.

[86] S. Kobayashi, F. Komori, Y. Ootuka and W. Sasaki, J. Phys. Soc. Jpn. 49 (1980) 1635.
[87] L. Van den dries, C. Van Haesendonck, Y. Bruynseraede and G. Deutscher, Phys. Rev. Lett. 46 (1981) 565.
[88] R.S. Markiewicz and L.A. Harris, Phys. Rev. Lett. 46 (1981) 1149.
[89] Z. Ovadyahu, Phys. Rev. B24 (1981) 7439.
[90] C. Van Haesendonck, L. Van den dries and Y. Bruynseraede, Phys. Rev. B25 (1982) 5090.
[91] Z. Ovadyahu, S. Moehlecke and Y. Imry, Surf. Sci. 113 (1982) 544.
[92] D.Y. Sharvin and Y.V. Sharvin, JETP Lett. 34 (1981) 272; Pis'ma Zh. Eksp. Teor. Fiz. 34 (1981) 285.
[93] A.K. Bhatnagar, A.K. Saxena and B. Gallardo, Solid State Commun. 41 (1982) 83.
[94] C. Van Haesendonck, L. Van den dries, Y. Bruynseraede and G. Deutscher, Physica 107B (1981) 7.
[95] W.C. McGinnis, M.J. Burns, R.W. Simon, G. Deutscher and P.M. Chaikin, Proc. 16th Int. Conf. Low Temp. Phys. Los Angeles 1981, ed. W.G. Clark (North-Holland, Amsterdam, Los Angeles, 1981) p. 5.
[96] G. Bergmann, Phys. Rev. Lett. 48 (1982) 1046.
[97] G. Bergmann, Phys. Rev. B25 (1982) 2937.
[98] G. Bergmann, Phys. Rev. Lett. 49 (1982) 162.
[99] T. Kawaguti and Y. Fujimori, J. Phys. Soc. Jpn. 51 (1982) 703.
[100] D.V. Borodin, Y.I. Latyshev and F.Y. Nad, JETP Lett. 35 (1982) 249; Pis'ma Zh. Eksp. Teor. Fiz. 35 (1982) 201.
[101] H. Hoffman, F. Hofmann and W. Schoepe, Phys. Rev. B25 (1982) 5563.
[102] B.L. Altshuler, A.G. Aronov, B.Z. Spivak, D.Y. Sharvin and Y.V. Sharvin, JETP Lett. 35 (1982) 588; Pis'ma Zh. Eksp. Teor. Fiz. 35 (1982) 476.
[103] M.E. Gershenson, V.N. Gubankov and J.E. Juravlev, Pis'ma Zh. Eksp. Teor. Fiz. 35 (1982) 467; JETP Lett. 35 (1982) 467.
[104] Y.F. Komnik, E.I. Bukhshtab, A.V. Butenko and V.V. Andrievsky, Sol. State Commun. 44 (1982) 865.
[105] G. Bergmann, Z. Physik B48 (1982) 5.
[106] Y. Bruynseraede, M. Gijs, C. Van Haesendonck and G. Deutscher, Phys. Rev. Lett. 50 (1983) 277.
[107] G. Bergmann, Z. Phys. B49 (1982) 133.
[108] M.E. Gershenson and V.N. Gubankov, Sol. State Comm. 41 (1982) 33.
[109] D. Abraham and R. Rosenbaum, Phys. Rev. B27 (1983) 1413.
[110] M.E. Gershenson, V.N. Gubankov and Y.E. Zhuravlev, Solid State Commun. 45 (1983) 87.
[111] F. Komori, S. Kobayashi and W. Sasaki, J. Phys. Soc. Jpn. 52 (1983) 368.
[112] T. Kawaguti and Y. Fujimori, J. Phys. Soc. Jpn. 52 (1983) 722.
[113] S. Kobayashi, S. Okuma and F. Komori, J. Phys. Soc. Jpn. 52 (1983) 20.
[114] P.H. Woerlee, G.C. Verkade and A.G.M. Jansen, J. Phys. C16 (1983) 3011.
[115] G. Bergmann, Solid State Comm. 46 (1983) 347.
[116] G. Bergmann, Phys. Rev. B28 (1983) 515.
[117] J.T. Masden and N. Giordano, Phys. Rev. B27 (1983) 6522.
[118] M. Gijs, C. Van Haesendonck, Y. Bruynseraede and G. Deutscher, preprint.
[119] G. Deutscher, M. Gijs, C. Van Haesendonck and Y. Bruynseraede, preprint.
[120] F. Komori, S. Kobayashi and W. Sasaki, J. Mag. Magn. Mat. 35 (1983) 74.
[121] F. Komori, S. Kobayashi and W. Sasaki, J. Phys. Soc. Jpn. 52 (1983) 4306.
[122] R.S. Markiewicz and C.J. Rollins, Phys. Rev. B29 (1984) 735.
[123] S. Okuma, F. Komori, Y. Ootuka and S. Kobayashi, J. Phys. Soc. Jpn. 52 (1983) 2639.
[124] Z. Ovadyahu, J. Phys. C: Solid State Phys. 16 (1983) L845.
[125] H.R. Raffy, R.B. Laibowitz, P. Chaudhari and S. Maekawa, Phys. Rev. B28 (1983) 6607.
[126] P. Santhanam and D.E. Prober, preprint.
[127] A.E. White, R.C. Dynes and J.P. Garno, preprint.
[128] M.J. Burns and P.M. Chaikin, Phys. Rev. B27 (1983) 5924.
[129] N. Giordano, W. Gilson and D.E. Prober, Phys. Rev. Lett. 43 (1979) 725.
[130] N. Giordano, Phys. Rev. B22 (1980) 5635.
[131] V.N. Bogomolov, E.V. Kolla and Y.A. Kumzerov, Solid State Commun. 46 (1983) 383.
[132] A.C. Sacharoff, R.M. Westervelt and J. Bevk, preprint.
[133] J.B. Bieri, A. Fert, G. Creuzet and J.C. Ousset, Solid State Commun. 49 (1984) 849.
[134] Y. Koike, M. Okamura, T. Nakamomyo and T. Fukase, J. Phys. Soc. Jpn. 52 (1983) 597.
[135] D.J. Bishop, D.C. Tsuei and R.C. Dynes, Phys. Rev. Lett. 44 (1980) 1153.
[136] Y. Kawaguchi and S. Kawaji, J. Phys. Soc. Jpn. 48 (1980) 699.
[137] D.J. Bishop, D.C. Tsuei and R.C. Dynes, Phys. Rev. Lett. 46 (1981) 360.
[138] M.J. Uren, R.A. Davies and M. Pepper, J. Phys. C13 (1980) L985.
[139] Y. Kawaguchi and S. Kawaji, Proc. 15th Int. Conf. Physics of semiconductors, Kyoto, 1980, J. Phys. Soc. Jpn. 49, Suppl. A (1980) 983.
[140] M.J. Uren, R.A. Davies, M. Kaveh and M. Pepper, J. Phys. C14 (1980) L395.
[141] Y. Kawaguchi and S. Kawaji, Surf. Sci. 113 (1982) 505.

[142] M.J. Uren, R.A. Davies, M. Kaveh and M. Pepper, J. Phys. C: Solid State Phys. 14 (1981) 5737.
[143] D.J. Bishop, R.C. Dynes and D.C. Tsui, Phys. Rev. B26 (1982) 773.
[144] R.A. Davies and M. Pepper, J. Phys. C: Solid State Phys. 15 (1982) L371.
[145] R.A. Davies and M. Pepper, J. Phys. C: Solid State Phys. 16 (1983) L361.
[146] A.K. Savchenko, V.N. Lutskii and V.I. Sergeev, Pis'ma Zh. Eksp. Teor. Fiz. 36 (1982) 150; JETP Lett. 36 (1982) 185.
[147] D.A. Poole, M. Pepper and A. Hughes, J. Phys. C15 (1982) L1137.
[148] R.G. Wheeler, K.K. Choi, A. Goel, R. Wisnieff and D.E. Prober, Phys. Rev. Lett. 49 (1982) 1674.
[149] R.A. Davies, M. Pepper and M. Kaveh, J. Phys. C: Solid State Phys. 16 (1983) L285.
[150] R.A. Davies and M. Pepper, J. Phys. C: Solid State Phys. 16 (1983) L353.
[151] R.C. Dynes, Physica B and C 109 (1982) 1857.
[152] Y. Isawa, K. Hoshino and H. Fukuyama, J. Phys. Soc. Jpn. 51 (1982) 3262.
[153] S. Uchida, K. Okajima and S. Tanaka, Solid State Commun. 37 (1981) 799.
[154] B.L. Altshuler and A.G. Aronov, to be publ. in Modern Problems in Condensed Sciences.
[155] G. Bergmann, Phys. Rev. B28 (1983) 2914.
[156] J.S. Langer and T. Neal, Phys. Rev. Lett. 16 (1966) 984.
[157] B.L. Altshuler, A.G. Aronov and P.A. Lee, Phys. Rev. Lett. 44 (1980) 1288.
[158] G. Bergmann, Phys. Rev. Lett. 43 (1979) 1357.
[159] F. Komori, S. Kobayashi and W. Sasaki, J. Phys. Soc. Jpn. 51 (1982) 3136.
[160] A.M. Finkelstein, Zh. Eksp. Teor. Fiz. 84 (1983) 168; Sov. Phys. JETP 57 (1983) 97.
[161] M. Kaveh, M.J. Uren, R.A. Davies and M. Pepper, J. Phys. C: Solid State Phys. 14 (1981) 413.
[163] A. Schmid, Z. Physik 271 (1973) 251.
[164] E. Abrahamas, P.W. Anderson, P.A. Lee and T.V. Ramakrishnan, Phys. Rev. B24 (1981) 6783.
[165] G.F. Giuliani and J.J. Quinn, Phys. Rev. B26 (1982) 4421.
[166] G. Bergmann, Phys. Lett. 29A (1969) 492.
[167] G. Bergmann, Phys. Rev. B3 (1971) 3797.
[168] A. Schmid, Z. Physik 259 (1973) 421.
[169] H. Takayama, Z. Physik 263 (1973) 329.
[170] B. Keck and A. Schmid, J. Low Temp. Phys. 24 (1976) 611.
[171] W. Buckel and R. Hilsch, Z. Physik 138 (1954) 109.
[172] G. Bergmann, Solid State Commun. 49 (1984) 775.